Doctoral Thesis

Interfacial Evolution and Engineering on LiMO$_2$ (M = Co, Ni, Mn) Positive Electrodes for All-Solid-State Li-Ion Batteries Using Sulfide Solid Electrolytes

Sung Hoo Jung

Department of Energy Engineering

(Battery Science and Technology)

Graduate School of UNIST

2019

Interfacial Evolution and Engineering on LiMO$_2$ (M = Co, Ni, Mn) Positive Electrodes for All-Solid-State Li-Ion Batteries Using Sulfide Solid Electrolytes

Sung Hoo Jung

Department of Energy Engineering

(Battery Science and Technology)

Graduate School of UNIST

Interfacial Evolution and Engineering on LiMO₂ (M = Co, Ni, Mn) Positive Electrodes for All-Solid-State Li-Ion Batteries Using Sulfide Solid Electrolytes

A dissertation

submitted to the Graduate School of UNIST

in partial fulfillment of the

requirements for the degree of

Doctor of Philosophy

Sung Hoo Jung

05/31/2019
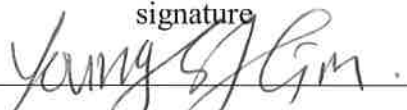
Approved by

Advisor

Youngsik Kim

Interfacial Evolution and Engineering on LiMO$_2$ (M = Co, Ni, Mn) Positive Electrodes for All-Solid-State Li-Ion Batteries Using Sulfide Solid Electrolytes

Sung Hoo Jung

This certifies that the dissertation of Sung Hoo Jung is approved.
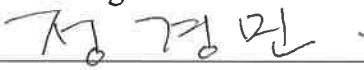
05/31/2019

signature

Advisor: Youngsik Kim

signature

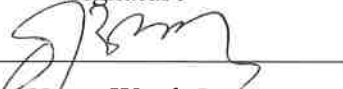Advisor: Yoon Seok Jung

signature

Kyeong-Min Jeong

signature

Seok Ju Kang

signature

Hyun-Wook Lee

Abstract

Most inorganic solid electrolytes (SEs) suffer from narrow intrinsic electrochemical windows and incompatibility with electrode materials, which results in the below par electrochemical performances of all-solid-state Li-ion or Li batteries (ASLBs). Unfortunately, in-depth understanding on the interfacial evolution and interfacial engineering via scalable protocols for ASLBs to mitigate these issues are at an infancy stage.

In this dissertation, rationally designed $Li_3BO_3-Li_2CO_3$ (or $Li_{3-x}B_{1-x}C_xO_3$ (LBCO)) coatings for $LiCoO_2$ (LCO) in ASLBs employing sulfide SE of Li_6PS_5Cl (LPSCl) were reported. The new aqueous-solution-based Li_3BO_3 (LBO) coating protocol allows us to convert the surface impurity on LCO, Li_2CO_3 into highly Li^+-conductive LBCO layers (6.0×10^{-7} S cm^{-1} at 30 °C for LBCO vs. 1.4×10^{-9} S cm^{-1} at 100 °C for Li_2CO_3 or 1.4×10^{-9} S cm^{-1} at 30 °C for LBO), which also offer interfacial stability with sulfide SE. By applying these high-surface-coverage LBCO coatings, significantly enhanced electrochemical performances are obtained in terms of capacity, rate capability, and durability. It is elucidated that the LBCO coatings suppress the evolution of detrimental mixed conducting interphases containing Co_3S_4 and effectively passivate the interfaces by the formation of alternative interface phases.

Contents

List of figures

incident ions.

Figure 12. Electrochemical characterization of $LiCoO_2$/Li−In all-solid-state cells at 30 °C. Charge−discharge voltage profiles for (a) LBO- and (b) LBCO-coated $LiCoO_2$ varied by C-rate. The results for c-bare, bare, and a-LBCO-coated (artificial-LBCO-coated) $LiCoO_2$ are compared in (a, b).

Figure 13. Electrochemical characterization of $LiCoO_2$/Li−In all-solid-state cells at 30 °C. Rate performances for (a) LBO- and (b) LBCO-coated $LiCoO_2$. The results for c-bare, bare, and a-LBCO-coated (artificial-LBCO-coated) $LiCoO_2$ are compared in (a−b).

Figure 14. Electrochemical characterization of $LiCoO_2$/Li−In all-solid-state cells at 30 °C. (a) Transient discharge voltage profiles obtained by GITT. (b) Nyquist plots of $LiCoO_2$/Li−In cells. The corresponding equivalent circuit model and interfacial resistances are shown in Figure 15 and Table 7, respectively.

Figure 15. Voigt-type equivalent circuit used for fitting the EIS data shown in Figure 14b.

Figure 16. Cycling performances for $LiCoO_2$/Li−In all-solid-state cells using c-bare, LBO-coated, and LBCO-coated $LiCoO_2$ at 0.2C and 30 °C. Discharge capacities as a function of the number of cycles in the voltage ranges of (a) 3.0−4.3 V (vs. Li/Li$^+$) and (b) 3.0−4.5 V (vs. Li/Li$^+$).

Figure 17. Thermodynamic calculation results for $LiNbO_3$ and electrochemical characterization of $LiNbO_3$-coated $LiCoO_2$ (1.0 wt%). a) Calculated mutual decomposition energy of Li_6PS_5Cl with $LiNbO_3$. b) Charge-discharge voltage profiles at 0.2C and 2C and cycle performance for $LiNbO_3$-coated $LiCoO_2$ in $LiCoO_2$/Li-In all-solid-state cells at 30 °C. The results for bare, LBO-coated, and LBCO-coated $LiCoO_2$ are compared.

Figure 18. XPS results of Co 2p signal for c-bare, LBO-coated (0.1 wt %), and LBCO-coated (0.5 wt % of LBO) $LiCoO_2$ for pristine powders and electrodes after cycling. The data for $LiCoO_2$/SE (Li_6PS_5Cl) mixtures is also shown for comparison.

Figure 19. XPS results of S 2p signal for c-bare, LBO-coated (0.1 wt %), and LBCO-coated (0.5 wt % of LBO) $LiCoO_2$ for electrodes after cycling. The data for $LiCoO_2$/SE (Li_6PS_5Cl) mixtures is also shown for comparison.

Figure 20. XPS results of P 2p signal for c-bare, LBO-coated (0.1 wt %), and LBCO-coated (0.5 wt % of LBO) $LiCoO_2$ for electrodes after cycling. The data for $LiCoO_2$/SE (Li_6PS_5Cl) mixtures is also shown for comparison.

Figure 21. Schematic diagram illustrating the different interface features of bare and LBCO-coated $LiCoO_2$ in all-solid-state-cell electrodes.

List of tables

Nomenclature

SE	Solid electrolyte
ASLB	All-solid-state lithium-ion battery
LBCO	Li_3BO_3-Li_2CO_3 or $Li_{3-x}B_{1-x}C_xO_2$
LCO	$LiCoO_2$
LPSCl	Li_6PS_5Cl
LBO	Li_3BO_3
LIB	Lithium-ion battery
LE	Liquid electrolyte
SEI	Solid electrolyte interphase
bcc	Body-centered cubic
LIPON	$Li_{3.3}PO_{3.9}N_{0.17}$
RT	Room temperature
LGPS	$Li_{10}GeP_2S_{12}$
LLZO	$Li_7La_3Zr_2O_{12}$
LLTO	$Li_{3x}La_{2/3-x/3}TiO_3$
LATP	$Li_{1.5}Al_{0.5}Ge_{1.5}(PO_4)_3$
LAGP	$Li_{1.4}Al_{0.4}Ti_{1.6}(PO_4)_3$
LISICON	Lithium super ionic conductor
a-LBCO	artificial-LBCO
c-bare	Cleaned bare
PEEK	Polyaryletheretherketone
GITT	Galvanostatic intermittent titration technique
XRD	X-ray diffraction
FESEM	Field emission scanning electron microscopy
BSE	Backscattered scanning electron
HRTEM	High-resolution transmission electron microscopy
STEM	Scanning transmission electron microscopy
EELS	Electron energy loss spectroscopy
XPS	X-ray photoelectron spectroscopy
TGA	Thermogravimetric analysis
LEIS	Low-energy ion scattering
SAED	Selected area diffraction
EIS	Electrochemical impedance spectroscopy
MCI	Mixed conducting interphase

1. Introduction

Over the past decades, rechargeable lithium-ion batteries (LIBs) have conquered the market of energy storage devices owing to their superior energy density to their competitors.   However, harsh efforts to maximize the energy density of LIBs, such as the use of ultra-thin separators (≤10 μm) and raising the upper limit of voltages, have brought unprecedented risks in safety, which originates from the use of flammable organic liquid electrolytes.[1-8]   Moreover, the safety concerns of LIBs are imperative for emerging large-scale applications, such as battery-driven electric vehicles and grid-scale energy storage.[9, 10]   In this regard, solidifying electrolytes with nonflammable inorganic materials is one of the best solutions.[10-16]   Additionally, inorganic solid electrolytes (SEs) are considered enablers for next-generation electrode materials, such as Li metal and S (or Li_2S), which typically suffer from poor compatibility with conventional organic liquid electrolytes.[10, 15-19]

Sulfide SE materials are some of the most promising candidates to realize high-performance all-solid-state batteries.   Several state-of-the-art sulfide superionic conductors developed (e.g., $Li_{10}GeP_2S_{12}$,[20] $Li_{9.54}Si_{1.74}P_{1.44}S_{11.7}Cl_{0.3}$,[11] $Li_7P_3S_{11}$[21]) have shown impressively high ionic conductivities reaching the order of 10^{-2} S cm^{-1} at room temperature with a single ionic transport nature, which implies the feasibility of all-solid-state batteries significantly outperforming conventional LIBs.[22, 23]   More importantly, sulfide materials are mechanically sinterable at room temperature and are thus beneficial for practical electrode fabrication.[10, 24]

Recent theoretical studies showed that similar to organic liquid electrolytes for conventional LIBs, inorganic SE materials also have narrow intrinsic electrochemical windows, and that the passivation of SEs is necessary for the reversible operation of all-solid-state batteries.[25-29]   In particular, the adaptation of conventional Li_xMO_2 (M = Co, Ni, Mn) cathode materials to all-solid-state Li-ion or Li batteries (ASLBs) suffers from huge interfacial resistances, which could be attributed to multiple factors such as surface impurities on Li_xMO_2,[30] severe reactions between Li_xMO_2 and sulfide SEs,[25, 29, 31] space charge layer effects,[32] lattice mismatches,[33] and poor wetting of SEs.[12, 13, 34]   It is known that the formation of surface impurities, such as LiOH and Li_2CO_3 on Li_xMO_2 in ambient atmosphere conditions, causes the degradation of the electrochemical performances of conventional LIBs.[35-37]   When it comes to ASLBs, the poor ion-conducting properties of the surface impurities could be more problematic.[30, 38] Since the first report in which it was demonstrated that interfacial engineering on $LiCoO_2$ using $Li_4Ti_5O_{12}$ could significantly lower the interfacial resistances in ASLBs,[32] various protective coatings have been developed (Table 1) to date: $LiNbO_3$,[11, 12, 39] Li_2SiO_3,[31] Ta_2O_5,[40] Al_2O_3,[41] and Li_3PO_4.[42]   In most previous works regarding ASLBs using Li_xMO_2 and sulfide SEs, Li_xMO_2 coated with these materials were tested without placing a strong emphasis on the mechanistic details of the coatings.[10-12, 14, 20, 23, 24, 34]   Moreover, to date, only a few in-depth and/or systematic studies on Li_xMO_2/SE interfacial evolution/engineering have been reported.[29, 31, 42-44]   The general consensus from the previous reports

is that the interfacial resistance of ASLBs is inversely proportional to the Li^+ conductivity of the coating materials.[42]   For example, using an amorphous $Li_{3.5}Si_{0.5}P_{0.5}O_4$ coating with a high Li^+ conductivity of 1.6×10^{-6} S cm^{-1} at room temperature resulted in a promising electrochemical performance of $LiCoO_2/In$ ASLBs,[42] though the high ionic conductivity of the coating material could be achieved only for its amorphous form, derived by a costly vacuum deposition process. $LiNbO_3$ is one of the most frequently practiced coating materials for sulfide ASLBs because of its high Li^+ conductivity of $\sim10^{-6}$ S cm^{-1} at room temperature and easy preparation protocol based on a wet method using alcohols (Table 1).[10-12, 14, 20, 23, 24, 34, 39]   However, Nb is not earth-abundant and the use of flammable alcohol in the coating process would be a concern when scaling up.   While these findings on the correlation between the Li^+ conductivity of the coating materials and the electrochemical performance aid in the design of alternative coating materials, it should be noted that the multiple aspects of not only Li^+ conductivity, but also scalable preparation and cost-effectiveness should be carefully considered.   Moreover, a detailed understanding on the evolution at electrode-SE interfaces affected by protective coatings is required.   These aspects are imperative for the practical development of high-performance ASLBs.

  From this background, Li_3BO_3 (LBO) has caught our attention.   Despite its relatively low Li^+ conductivity (1.4×10^{-9} S cm^{-1} at 30 °C, measured in this work), LBO has been investigated as a sintering aid for oxide SE materials, such as $Li_7La_3Zr_2O_{12}$, for oxide-based ASLBs, as it can help lower the sintering temperatures for the oxide SEs because of its low melting point (700 °C).[45-50] However, until now, there has been no report on the application of LBO or LBO-derived materials for sulfide-based ASLBs. Herein, we report the development of rationally designed Li_3BO_3-Li_2CO_3 (LBO-LCO or $Li_{3-x}B_{1-x}C_xO_3$ (LBCO)) protective coatings prepared via a simple and scalable wet protocol using water, which drastically enhances the electrochemical performances of $LiCoO_2$ for ASLBs using sulfide SEs.   The surface impurity on $LiCoO_2$, Li_2CO_3, generally impedes Li^+ transport at the interfaces, but, after the aforementioned wet-coating process for LBO, it is converted into highly Li^+ conductive LBCO coating layers.   Complementary analyses reveal that the as-derived highly conductive, thick, and high-surface-coverage LBCO coatings for $LiCoO_2$ effectively suppress the formation of detrimental Co_3S_4 phase and form good passivating layers comprised of phosphates, thus minimizing interfacial resistances.   This is also supported by our thermodynamic computational results based on first principles calculations regarding various states of mixed phases.   Compared with other coating materials, LBCO and its precursor are cost-effective and environmentally benign (Table 1).   Moreover, the use of water as a solvent is a significant advantage which avoids the use of flammable solvents employed in typical coating procedures.

Table 1. Characteristics of various coating materials for $LiCoO_2$ for ASLBs.

Material	σ_{RT} [S cm^{-1}]	Crystallinity	Preparation method			Price [USD/ton][c]	Ref
			Reported method	Availability of wet-method	Solvent		
$Li_4Ti_5O_{12}$	-	-	Wet method	O	EtOH	2.5–2.8 k (TiO$_2$) 3.5–3.6 k (Ti(OiPr)$_4$)	32
$LiNbO_3$	~10^{-6}	Low	Wet method	O	EtOH	120–180 k (Nb$_2$O$_5$) 1000–1500 k (Nb(OEt)$_5$)	39
Ta_2O_5	10^{-6}		Solid-state reaction followed by wet-method	Δ	-	169–390 k (Ta$_2$O$_5$)	40
$LiTaO_3$	~10^{-6}	Low			-	169–390 k (Ta$_2$O$_5$)	51
$Li_{56}Nb_{22}Ta_{22}$ oxide	4.2×10^{-6}	Low	Physical vapor deposition	Δ	-	169–390 k (Ta$_2$O$_5$)	51
Li_4SiO_4	1×10^{-8}	Low	Pulsed laser deposition	Difficult	-	3.2–4.0 k (SiO$_2$)	42
Li_4GeO_4	7×10^{-8}	Low	Pulsed laser deposition	Difficult	-	900–1200 k (GeO$_2$)	42
$Li_{3.5}Ge_{0.5}P_{0.5}O_4$	2×10^{-7}	Low	Pulsed laser deposition	Difficult	-	900–1200 k (GeO$_2$)	42
Li_3PO_4	5×10^{-7}	Low	Pulsed laser deposition	Difficult	-	0.7–0.9 k (H$_3$PO$_4$)	42
$Li_{3.5}Si_{0.5}P_{0.5}O_4$	10^{-6}	Low	Pulsed laser deposition	Difficult	-	3.2–4.0 k (SiO$_2$)	42
Al_2O_3	-	Low	Atomic layer deposition	O	EtOH	0.4–0.6 k (Al$_2$O$_3$)	41
$Li_2O\text{-}ZrO_2$	~10^{-9a}	-	Wet method	O	Propanol	15–30 k (ZrO$_2$) 100 k (Zr(OPr)$_4$)	52
Li_3BO_3	1×10^{-9} $(2 \times 10^{-8})^b$	High	Wet method	O	Water	0.6–0.8 k (H$_3$BO$_3$)	This work
$Li_{3-x}B_{1-x}C_xO_3$	6×10^{-7} $(1.2 \times 10^{-6})^b$	High	Wet method	O	Water	0.6–0.8 k (H$_3$BO$_3$)	This work

[a] Obtained using the sample prepared by solid-state synthesis. [b] Glass-ceramic prepared by solid-state synthesis. [c] From https://www.alibaba.com

2. Background

2.1. Principle of lithium-ion secondary batteries

Lithium-ion secondary batteries (LIBs) are energy storage devices that store electrical energy as chemical energy and convert chemical energy into electrical energy when needed.[53] LIBs are made up of four major components: cathode active material, anode cathode material, electrolyte and separator. The schematic illustration of the LIBs is shown in Figure 1.[54] The electrolyte and separator, which allows lithium to move and pass through, respectively, cannot move and pass through electrons. So, they can separate the lithium-ion pathway from the electron pathway between the two electrodes; Lithium-ion moves inside a cell and electrons move to an external wire to create electrical energy.[54] LIBs were first commercialized in 1991 using the cathode material, $LiCoO_2$ and anode material graphite. The working voltage difference of lithium-ion batteries between the cathode and the anode is superior to other batteries, resulting in much higher energy.[53, 54] However, the electrolyte decomposition reaction is inevitable because the electrochemical window of the organic liquid electrolytes used is narrower than the high voltage difference between cathode and anode. Fortunately, electrolyte decomposed products can make solid electrolyte interphase (SEI), a layer that can pass through lithium ion but cannot pass through electrons, to prevent further electrolyte decomposition reactions when the battery is driven. This allows us to re-charge and reuse lithium-ion secondary batteries that produce high energy several times.

Recently, higher energy density and power density of LIBs are required as lithium secondary batteries become larger. Minimizing the thickness of the separation film, not the energy-producing material, can greatly help increase the energy densities, but this resulted in stability problems. Not only is LIBs storing high energy, but it also contains all three elements of combustion inside the battery, so stability problems cannot be eliminated fundamentally.[1-8]
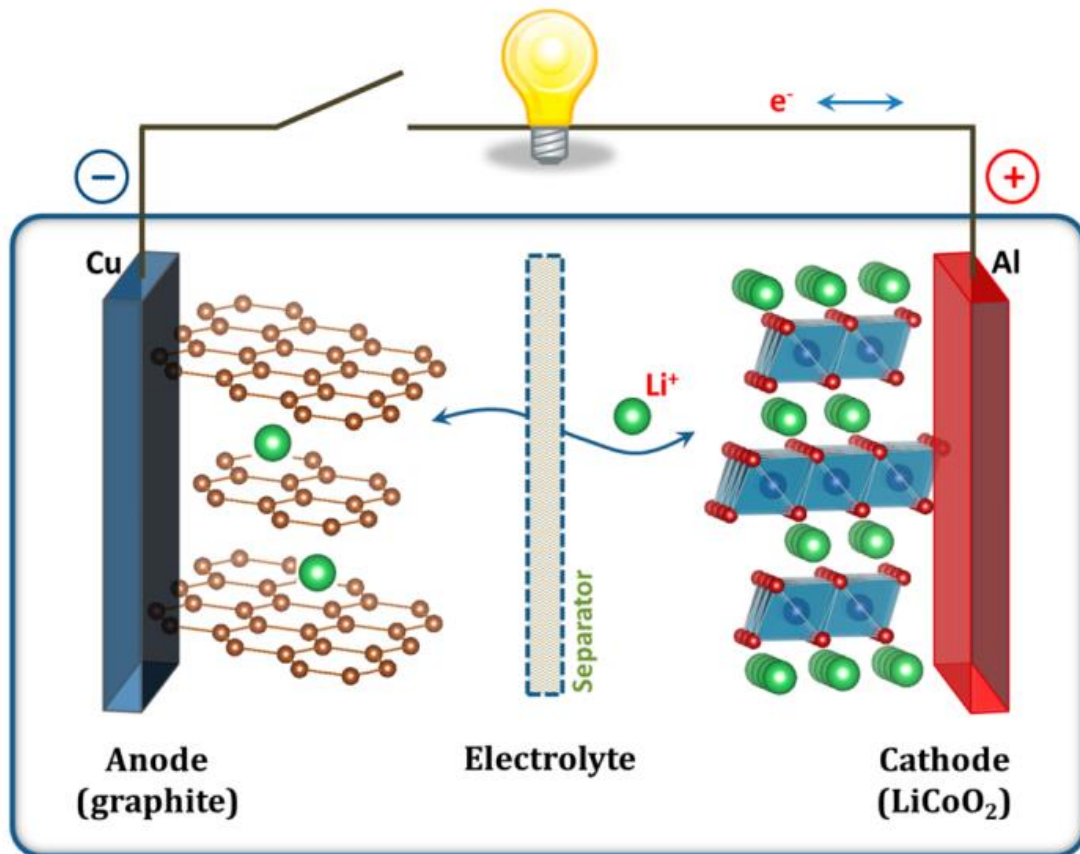
Figure 1. Schematic illustration of the first Li-ion battery ($LiCoO_2/Li^+$ electrolyte/graphite). Copyright 2013, ACS publications

2.2. All-solid-state Lithium-Ion batteries

All-solid-state Lithium-ion Batteries (ASLBs) are the batteries that replace organic liquid electrolytes (LEs) in conventional lithium-ion batteries with solid electrolytes. LEs account for most of the aforementioned three combustion elements inside the battery. But, replacing them with solid electrolytes brings ultimate safety.[10-16] In addition, ASLBs have lots of possibilities of showing up high energy density and power density. Because all components of battery including electrolytes are solid, cells can easily be stacked without any external pouch as there is no leakage concern.[11] In addition, the heat management system can be minimized. High energy materials such as Li and S have had difficulty in commercializing in the conventional LIBs can also solve safety concerns and dissolution problems respectively in ASLBs.[10, 15-19] These differences have great potential for improving the energy density of ASLBs. The power densities are expected to be greatly improved. The SEs having higher Li^+ ion conductivity than LEs have been developed even though the development of ASLBs is shorter than that of LIBs. The SEs also has a lithium transfer number of 1, so there is no concern about the movement of the bulky negative ion that exists in liquid electrolytes.[10-16] Solid electrolytes have excellent thermal stability, enabling elevated temperature (>70 °C) that was not possible in conventional LIBs.[11] Thanks to these potentials, interest in ASLBs is now greatly increased and lots of research is underway.

2.2.1. Solid electrolytes

Typical solid electrolytes used in ASLBs are divided into oxide-based, sulfide-based and polymer-based SEs, and research regarding halide and hydride-based SEs also has been actively carried out recently. The requirements of good SEs include 1) high Li-ion conductivity, 2) wide electrochemical window (oxidation and reduction stability), 3) high deformability, 4) chemical stability, and 5) cheap processing cost. The performance characteristics of each SEs are shown in in Figure 2.[55]

Li ion transport in solid electrolyte crystals is an important process of the overall charge transfer reaction of ASLBs.[56] Three factors, such as carrier type, diffusion path and diffusion type, control the Li ion transport mechanism within the solid electrolyte. Carrier types are closely related to defect chemistry. The diffusion path has a large correlation with the anion arrangement.[57] It has been proposed that an anion sublattice having a structure similar with body centered cubic (bcc) having a low energy barrier is more advantageous for Li-ion diffusion than another close-packed framework.[57] The Li ion diffusion type also affects the ionic conductivity and has three types; direct interstitial hopping, interstitial knock-off and direct vacancy hopping.[56]

2.2.2. Bulk-type all-solid-state lithium-ion batteries

Thin-film ASLBs using $Li_{3.3}PO_{3.9}N_{0.17}$ are well known as commercial batteries with excellent performance. However, the use of thin film ASLB is limited to small applications such as smart cards and microelectronics devices due to the expensive vacuum deposition process required for production. [58-60] Recently, ASLBs as not only portable electronic devices but also large-scale batteries are drawing attention. [61, 62] As shown in Figure 3, an important feature of bulk-type ASLB is the composite electrode structure including active materials, conductive materials and SEs Bulk-type ASLBs don't need to be produced by expensive vacuum deposition processes unsuitable for large applications. [14] In bulk-type ASLB, SE particles replace the conventional LE of the LIBs. Thick composite electrodes of ASLBs indicate that increased energy density can compete with conventional LIBs, but this requires high ion conductivity of SEs that comparable to that of LEs. Until now, many SEs have been developed with a conductivity of 10^{-4}-10^{-2} S cm^{-1} at room temperature (RT). The oxide-based and sulfide-based SEs have been extensively investigated as suitable SEs for bulk-type ASLBs. Especially, the most important advantage of sulfide SE over oxide SE is that the SE powders can be easily transformed to pellet form simply by cold pressing not contain any other heat treatment. [10, 14]
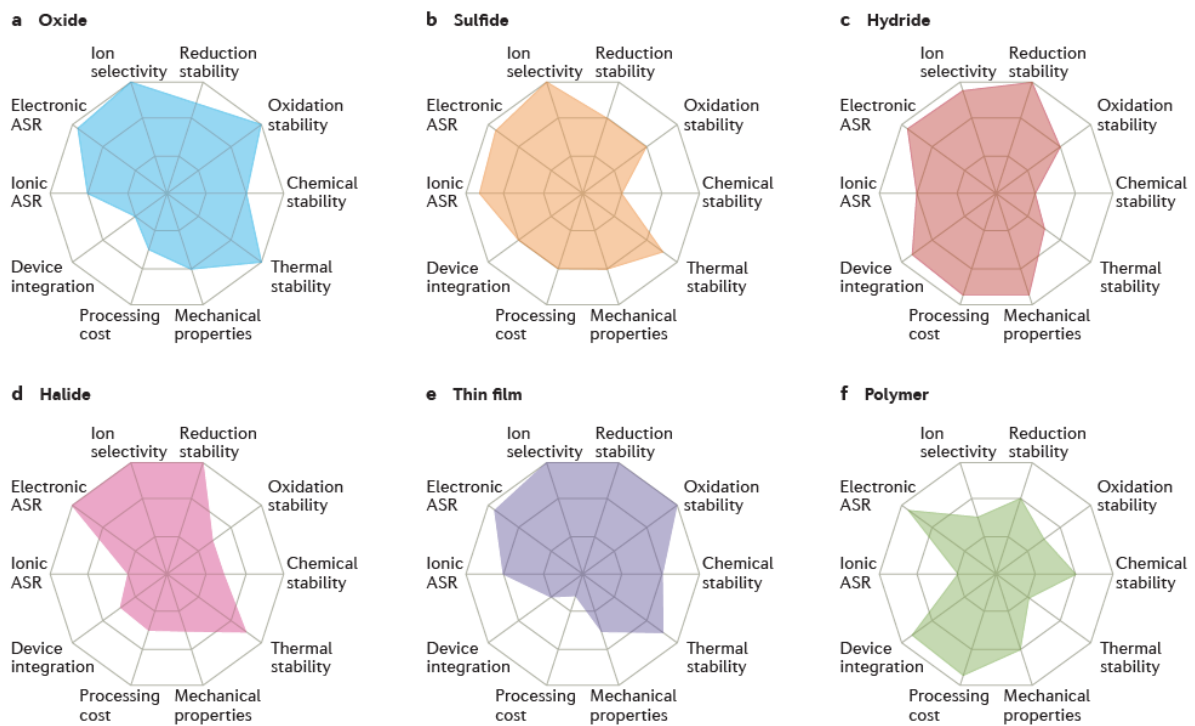
Figure 2. Performance of different solid electrolyte materials. Radar plots of the performance properties of oxide solid electrolytes (panel a), sulfide solid electrolytes (panel b), hydride solid electrolytes (panel c), halide solid electrolytes (panel d), thin-film electrolytes (panel e) and polymer solid electrolytes (panel f). ASR, area-specific resistance. Copyright 2017, Springer Nature
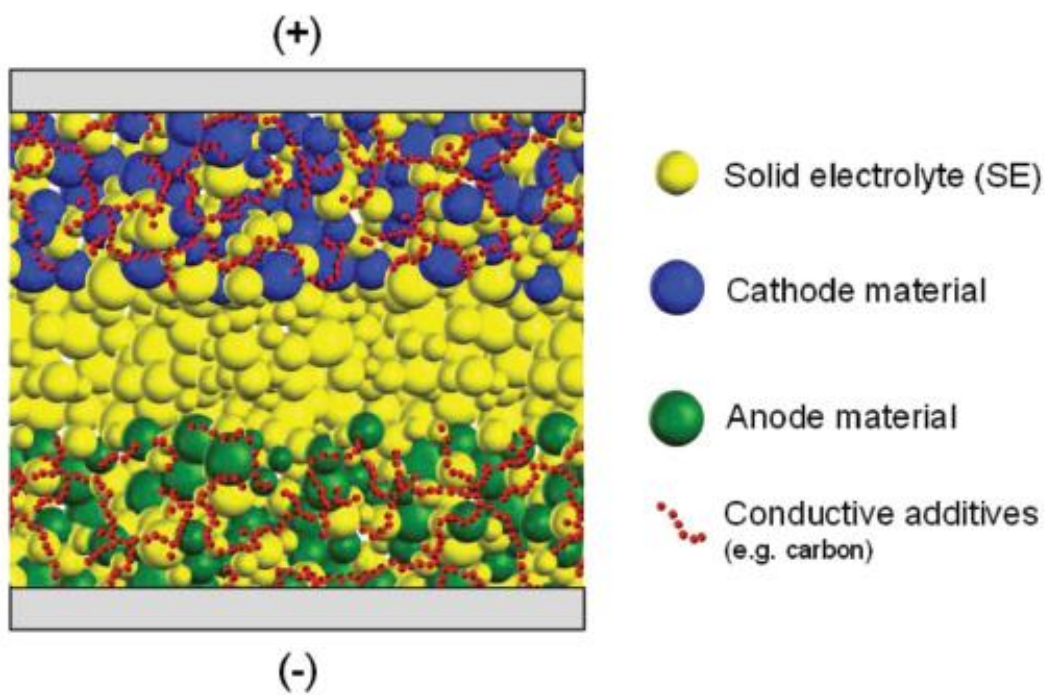
Figure 3. Schematic diagram of bulk-type all-solid-state batteries. Copyright 2018, Wiley-VCH

2.2.3. Interfacial issues for bulk-type all-solid-state lithium-ion batteries

A very wide electrochemical stability window (0.0–5.0 V) is required for the ideal SEs to combine lithium metal anodes with high voltage cathode material to activate the highest voltage output of ASLBs. Electrochemical window of SEs was generally obtained by applying cyclic voltammetry to Li/SE/metal semi-blocking cells. As a result of testing with this method, very wide electrochemical window from 0V to 5V was reported to most sulfide and oxide SEs.[20, 63] However, the electrochemical performance of bulk-type ASLBs assembled with these SEs is much worse than conventional LIBs based on LEs, even though SEs have high ion conductivity that can be compared with liquid electrolytes.[20, 31] Recent thermodynamic calculations indicate that SEs have very narrow electrochemical windows, unlike conventional experimental results (Table 2).[25, 27]

High interfacial resistance is often insisted as a major limiting factor in the performance of ASLBs.[64] Although not yet fully understood, the origin of interfacial resistance is often due to physical interfacial contact,[12] formation of space charge layers,[65] and/or formation of mutual interphase layers due to chemical/electrochemical reactions between electrolytes and electrodes.[27, 28, 32, 44, 50] Although various interface processing techniques such as dynamic pressing,[12] nanosizing,[66] co-sintering[67] and surface coating[12, 32, 39] have attempted to engineer interfaces between electrode materials and SEs, the performance of ASLBs is still significantly lower than that of a conventional LIBs. Understanding and resolving the interfacial problems between electrode materials and SEs will be the key to exceeding the performance of the conventional LIBs.

Table 2. Electrochemical window and phase equilibria at the reduction and oxidation potentials of the solid electrolyte materials. Copyright 2015, ACS publications

	Reduction Potential (V)	Phase equilibria at the reduction potential	Oxidation potential (V)	Phase equilibria at the oxidation potential
Li_2S	-	Li_2S (stable at 0 V)	2.01	S
$Li_{10}GeP_2S_{12}$	1.71	P, Li_4GeS_4, Li_2S	2.14	Li_3PS_4, GeS_2, S
$Li_{3.25}Ge_{0.25}O_{0.75}S_4$	1.71	P, Li_4GeS_4, Li_2S	2.14	Li_3PS_4, GeS_2, S
Li_3PS_4	1.71	P, Li_2S,	2.31	S, P_2S_5
Li_4GeS_4	1.62	Li_2S, Ge	2.14	GeS_2, S
$Li_7P_3S_{11}$	2.28	Li_3PS_4, P_4S_9	2.31	S, P_2S_5
Li_6PS_5Cl	1.71	P, Li_2S, LiCl	2.01	Li_3PS_4, LiCl, S
$Li_7P_2S_8I$	1.71	P, Li_2S, LiI	2.31	LiI, S, P_2S_5
LIPON	0.68	Li_3P, $LiPN_2$, Li_2O	2.63	P_3N_5, $Li_4P_2O_7$, N_2
LLZO	0.05	Zr_3O, LaO_3, Li_2O	2.91	Li_2O_2, La_2O_3, $Li_6Zr_2O_7$
LLTO	1.75	$Li_4Ti_5O_{12}$, $Li_{7/6}Ti_{11/6}O_4$, $La_2Ti_2O_7$	3.71	O_2, TiO_2, $La_2Ti_2O_7$
LATP	2.17	P, $LiTiPO_5$, $AlPO_4$, Li_3PO_4	4.21	O_2, $LiTi_2(PO_4)_3$, $Li_4P_2O_7$, $AlPO_4$
LAGP	2.70	Ge, GeO_2, $Li_4P_2O_7$	4.27	O_2, $Ge_5O(PO_4)_6$, $Li_4P_2O_7$, $AlPO_4$
LISICON	1.44	Zn, Li_4GeO_4	3.39	Li_2ZnGeO_4, Li_2GeO_3, O_2

3. Experimental

3.1. Preparation of materials

The LBO and LBCO powders were prepared by dissolving a stoichiometric amount of LiOH (99.995%, Alfa Aesar), H_3BO_3 (>99.5%, Sigma-Aldrich), and Li_2CO_3 (99.997%, Sigma-Aldrich) in deionized water. The water was evaporated under a vacuum at 60 °C using a rotary evaporator, followed by a heat treatment at 600 °C for 5 h in air. The cleaned bare $LiCoO_2$ powders (c-bare) were prepared by heat treatment at 600 °C for 10 h in air. The LBO- and LBCO-coated $LiCoO_2$ powders were prepared using an aqueous LBO solution. After the bare $LiCoO_2$ powders were added into the coating solution prepared by dissolving a stoichiometric amount of LiOH (99.995%, Alfa Aesar) and H_3BO_3 (>99.5%, Sigma-Aldrich) in deionized water, the solvent was evaporated under a vacuum at 60 °C using a rotary evaporator, followed by a heat treatment at 600 °C for 10 h in air. To obtain the LBO- and LBCO-coated $LiCoO_2$ powders, c-bare and bare $LiCoO_2$ powders were used, respectively. For the LBCO-coated $LiCoO_2$ powders, the surface impurity, Li_2CO_3, serves as the source for the coating materials. In contrast, the artificial-LBCO-coated (a-LBCO) $LiCoO_2$ powders were prepared using c-bare $LiCoO_2$ and a coating solution, prepared by dissolving LiOH, H_3BO_3, and Li_2CO_3 (99.997%, Sigma-Aldrich) in deionized water. The LPSCl SE powders were prepared by ball milling a stoichiometric mixture of Li_2S (99.9%, Alfa Aesar), P_2S_5 (99%, Sigma-Aldrich), and LiCl (99.99%, Sigma-Aldrich) at 600 rpm for 10 h with ZrO_2 balls.[23] Then, the ball-milled powders were heat-treated at 550 °C for 5 h in an Ar atmosphere.

3.2. Thermodynamic calculations

Potential reactions at the interfaces were considered as chemical reactions between two corresponding compositions at the interfaces.[27, 28] Multi-dimensional compositional phase diagrams were constructed, and then pseudo-binary phase diagrams that have the two target compositions as end points were extracted from the multi-dimensional phase diagrams. The potential decomposition reactions were examined along the pseudo-binary phase diagrams with varying fractions of reactants. Most of the energy values used for constructing phase diagrams were obtained from the Materials Project database.[68] However, the energies of unstable target materials, such as layered $Li_{0.5}CoO_2$ and Li_6PS_5Cl, were corrected by making their decomposition energies become zero, as previously suggested.[25] Additionally, the energy of LBCO ($Li_{3-x}B_{1-x}C_xO_3$, x = 0.80) was evaluated as a linear combination of Li_3BO_3 and Li_2CO_3 because calculating the exact energy of the phase is computationally impossible. Despite these assumptions, we believe that the error of the calculated decomposition energy does not significantly affect the outcome of this study.

3.3. Materials characterization

The XRD measurements were conducted using a D8-Bruker Advance diffractometer under Cu K_α radiation (1.54056 Å).   To avoid exposure to air, the samples were sealed with a Be window.   The FESEM and BSE measurements were carried out using Quanta 200FEG (FEI).   The accelerating voltage and emission current were fixed at 1 kV and 10.5 μA, respectively.   The HRTEM images and their corresponding selected-area electron diffraction (SAED) patterns and EELS spectra were obtained using JEM-2100 (JEOL) and JEM-2100F (JEOL).   The XPS data were collected with a monochromatic Al K_α source (1486.6 eV) at 72 W, 12 kV, and 6 mA using an X-ray photoelectron spectrometer (ThermoFisher).   For the ex-situ XPS measurements, the collected samples were loaded in an Ar-filled dry glove box and loaded into the XPS equipment shortly while minimizing exposure to air.   The TGA measurements were conducted using Q500 (TA Instrument Corp.).   The weight fraction of the coating materials was determined using inductively coupled plasma optical emission spectroscopy (ICP-OES, 720-ES, Varian).   The LEIS measurements were carried out using Qtac100 (IONTOF GmbH).

3.4. Electrochemical characterization

For the measurement of Li^+ conductivity, LBO and LBCO pellets were prepared by cold-pressing of the powders at 370 MPa and subsequent sintering at 600 °C for 10 h in air.   The as-prepared pellets were subjected to measurements of Li^+ conductivity by the AC impedance method (Iviumstat, IVIUM Technologies Corp.) using symmetric Li-ion blocking carbon-coated Al (c-Al)/pellet/c-Al cells.   The $LiCoO_2$/Li-In all-solid-state cells were prepared as follows.[12, 23]   Partially lithiated indium ($Li_{0.5}In$, nominal composition) powders were prepared by mechanically milling a mixture of In (Sigma Aldrich, 99.99%) and Li (FMC Lithium corp.).   After the SE layer was formed by pressing 150 mg of LPSCl powders, the electrode mixtures of $LiCoO_2$ and LPSCl (70:30 weight ratio) were spread on one side of the SE layer, followed by pressing.   Then, the as-prepared $Li_{0.5}In$ powders were put on the other side of the SE layer.   Finally, the whole assemblies were pressed at 370 MPa.   The mass loading of $LiCoO_2$ was 8.3 mg cm^{-2}.   All the pressing was carried out in a polyaryletheretherketone (PEEK) mold (diameter = 13 mm) with Ti rods as current collectors.   All the electrochemical tests were conducted at 30 °C.   The C-rate of 1C corresponds with 161 mA g^{-1}.   The GITT measurements were carried out at a pulse current of 0.5C for 90 s and a rest for 2 h.   The EIS measurements were performed from 1.5 MHz to 5 mHz with 10 mV of amplitude after discharging the cells to 3.9 V (vs. Li/Li^+) at 0.2C at the second cycle.

4. Results and Discussion

4.1. Thermodynamic calculations of coating materials

In our screening process for potential coating materials, we first carried out computational investigations to examine the intrinsic interfacial stability between the cathode and SE material, along with the effects of applying coating materials on it. First, the electrochemical window and possible oxidized products of SE and coating materials were calculated in Table 3. Various possible reactions at the interfaces before and after introducing coating materials were probed by calculating the thermodynamic reaction energies, as illustrated in Figure 4. The blue dashed line in the Figure presents the interfacial reaction energy as a function of the atomic fraction of the SE materials (Li_6PS_5Cl (LPSCl)) surrounding the cathode ($LiCoO_2$), which models the various local compositional inhomogeneities in the composite electrode. These analyses reveal that the interface between the cathode and SE material is not intrinsically stable, but undergoes a spontaneous decomposition with negative reaction energy, which becomes maximum (-320 meV atom^{-1}) when LPSCl and $LiCoO_2$ react at a ratio of approximately 1:1. Moreover, the decomposition reaction is further promoted when the SE materials are in contact with the delithiated cathode ($Li_{0.5}CoO_2$), with a maximum energy of -450 meV atom^{-1}, as displayed by the red dashed line, indicating more serious side reactions during the charging of ASLBs. This decomposition reaction deteriorates the interface properties and often leads to an increase of cell impedance and the loss of active materials in the electrochemical reaction. However, we observed that the stability of the SE can be significantly enhanced when it is alternatively in contact with coating materials, such as LBCO or LBO. The solid lines show that the decomposition of electrolytes can be mitigated by coating layers with a substantially reduced reaction energy. Even though the decomposition reaction is still thermodynamically favorable, the driving force is reduced by less than one fifth. Moreover, the interfaces between $LiCoO_2$ and LBCO (or LBO) were found to be stable without decomposition or with negligible decomposition energies (Table 4), which indicates that the surface degradation of $LiCoO_2$ can be suppressed by incorporating LBCO (or LBO) as coating layers. As a result, the incorporation of LBCO (or LBO) as a coating layer is expected to suppress the decomposition reactions of both the cathode and the SE materials at the interface of them.

Table 3. Intrinsic electrochemical window and oxidation reaction of SE and coating materials

Sample	Electrochemical window [V $vs.$ Li/Li$^+$]	Reaction at oxidation potential
LPSCl	1.72-2.14	$Li_6PS_5Cl \rightarrow Li_3PS_4 + 0.25LiS_4 + LiCl + 1.75Li$
LBO	0.28-3.47	$Li3BO3 \rightarrow 0.25Li6B4O9 + 0.345O2 + 1.5Li$
LBCO	1.27-3.47	$Li_{2.2}B_{0.2}C_{0.8}O_3 \rightarrow 0.05Li_6B_4O_9 + 0.8Li_2CO_3 + 0.075O_2 + 0.3Li$
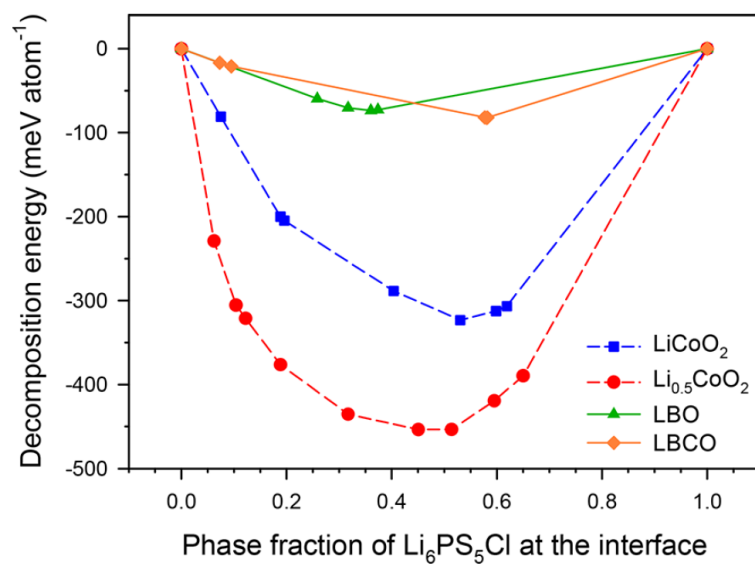
Figure 4. Calculated mutual decomposition energy of Li_6PS_5Cl with pristine and delithiated $LiCoO_2$, LBO (Li_3BO_3), and LBCO ($Li_{3-x}B_{1-x}C_xO_3$, x = 0.80) at various phase fractions of Li_6PS_5Cl in the mixed compounds.

Table 4. Calculated maximum mutual decomposition energy of the coating materials with pristine and delithiated $LiCoO_2$.

Sample	$LiCoO_2$	$Li_{0.5}CoO_2$
LBO	No reaction	-4.4 meV atom^{-1}
LBCO	No reaction	-1.5 meV atom^{-1}

4.2. Characterization of coating materials and coated active materials

Inspired by the computational results, a series of LBCO-coated $LiCoO_2$ samples were prepared, along with the reference samples of $Li_{3-x}B_{1-x}C_xO_3$. The reference $Li_{3-x}B_{1-x}C_xO_3$ samples were obtained from a homogeneous aqueous solution containing LiOH, H_3BO_3, and Li_2CO_3. The phase-pure LBO samples (JCPDS no. 18-0718, Fig. S1a) exhibited a Li^+ conductivity of 1.4×10^{-9} S cm^{-1} at 30 °C (Figure 5, Table 5).[49] As Li_2CO_3 is added into LBO, the characteristic peaks for the isostructural phase with Li_2CO_3 (JCPDS no. 22-1141) evolved, as seen in the XRD patterns (Figure 6).[49, 69] Correspondingly, Li^+ conductivity was drastically increased to 6.0×10^{-7} S cm^{-1} at x = 0.80 (Figure 5, Table 5), which is comparable to that of the state-of-the-art coating material for sulfide ASLBs: amorphous $LiNbO_3$ (Table 1).[11, 12, 39] LBO-coated $LiCoO_2$ was fabricated using surface-cleaned $LiCoO_2$, referred to as "c-bare", which was obtained by a heat treatment at 600 °C in air, while the LBCO-coated $LiCoO_2$ was obtained using impurity-containing bare $LiCoO_2$, referred to as "bare". The characteristics of the LBO and LBCO coatings (weight fraction, thickness, and surface coverage) are provided in Table 6. Field emission scanning electron microscopy (FESEM) images of c-bare, LBO-coated (0.5 wt.%), and LBCO-coated (0.5 wt.% of LBO or 1.72 wt.% of LBCO) $LiCoO_2$ particles (Figure 7a-c, 8) showed no noticeable differences. However, the corresponding backscattered scanning electron (BSE) images reveal the inhomogeneous distribution of contrast in atomic numbers (Figur. 7a-c, 8), confirming the presence of the coating layers for LBO- and LBCO-coated $LiCoO_2$. Although a direct observation of the coating layers by high-resolution transmission electron microscopy (HRTEM) was hindered by the vulnerability of the low atomic-number constituents to electron beams, HRTEM images for LBO- and LBCO-coated $LiCoO_2$ particles showed lattice fringes corresponding with LBO ((020) plane) and LBCO ((-202) plane), as shown in Figure 9a, b respectively. Moreover, the presence of boron in the form of Li_3BO_3 on the surface of LBO- and LBCO-coated $LiCoO_2$ was corroborated by scanning TEM (STEM) images (Figure 10) and their corresponding electron energy loss spectroscopy (EELS) peaks at ~193 eV (Figure 9c).[70] In addition, compared with LBO-coated $LiCoO_2$, LBCO-coated $LiCoO_2$ exhibited a stronger carbon signature centered at ~292 eV.[71]

The presence of boron in coated $LiCoO_2$ was also confirmed by X-ray photoelectron spectroscopy (XPS) data for B 1s signals (Figure 11a). Both LBO- and LBCO-coated $LiCoO_2$ samples showed peaks at 191.5 eV corresponding to B^{3+} for Li_3BO_3.[70] The surface impurity on $LiCoO_2$, Li_2CO_3, was quantified by thermogravimetric analysis (TGA) in N_2. Whereas the c-bare sample showed no weight loss up to 850 °C, the bare sample started to lose weight at 700 °C, which is indicative of the thermal decomposition of Li_2CO_3 (Figure 11b).[72] From the weight loss value, the amount of Li_2CO_3 on the surface of the bare sample was determined to be 1.1 wt.%. The thicknesses of the coating layers were estimated considering the surface area of $LiCoO_2$ powders obtained by N_2 adsorption-desorption isotherm measurements and are given in Table 6. Low-energy ion scattering (LEIS) measurements

were carried out to analyze the conformality of the coating layers on $LiCoO_2$.[73]   In LEIS, low-energy backscattered ions are analyzed, allowing the identification and quantification of the elements in the outermost atomic layer of a substrate.[74]   Figure 11c shows the LEIS spectra for bare, c-bare, LBO-coated (0.5 wt.%), and LBCO-coated (0.5 wt.% of LBO) $LiCoO_2$ particles when using 5 keV Ne^+ as incident ions.   The strong peaks found at 1230 eV for the bare and c-bare samples correspond with the ions backscattered by Co in $LiCoO_2$.   The lower intensity of the Co peak obtained for the bare sample compared with that obtained for the c-bare sample is due to surface impurities containing Li_2CO_3. Furthermore, the LBO- and LBCO-coated samples showed a much more attenuated Co-peak, indicating that Co atoms are well covered by the coating layers.   Assuming that the surfaces of the c-bare sample are perfectly uncovered, the surface coverages of the other samples were determined by comparing the intensities of the Co peaks, and are shown in Table 6.   For the bare sample, 21% of the surface is covered by impurities, such as Li_2CO_3.   The surface coverages for LBO- and LBCO-coated samples turned out to be 79% and 87%, respectively.   The higher surface coverage found for the LBCO-coated sample than for the LBO-coated one is attributed to the overall larger amount of coating materials.
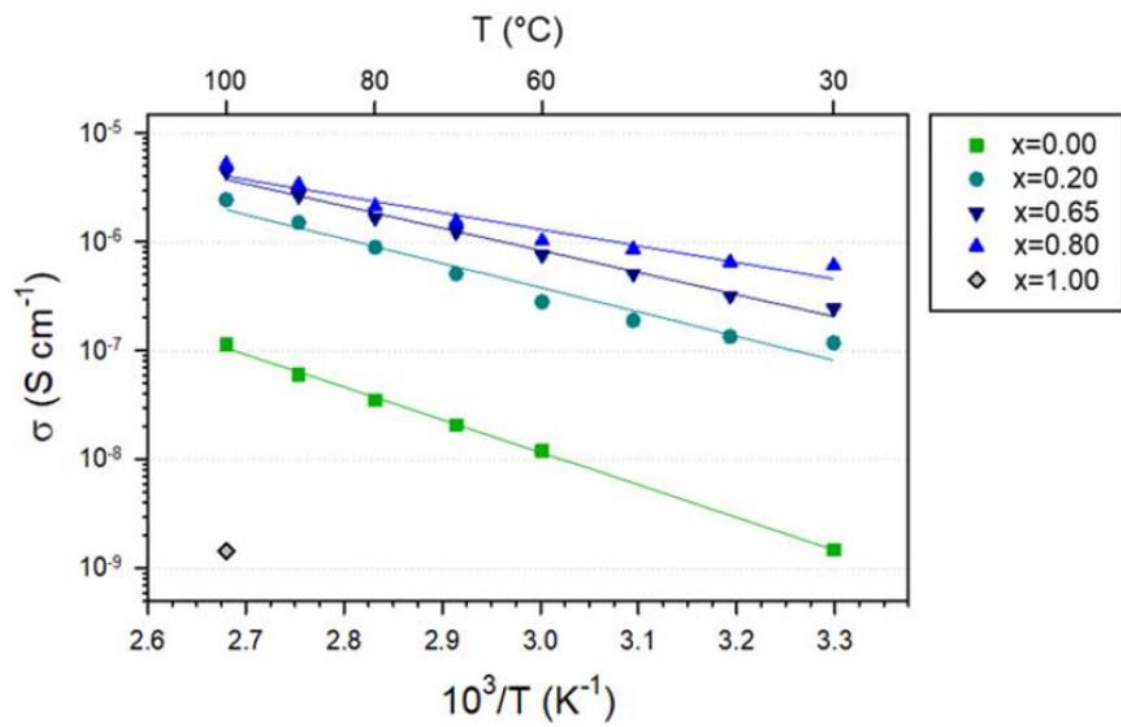
Figure 5. Arrhenius plots of Li^+ ion conductivities for $Li_{3-x}B_{1-x}C_xO_3$ (LBCO)

Table 5. Li$^+$ ion conductivity at 30 °C and activation energy of LBCO.

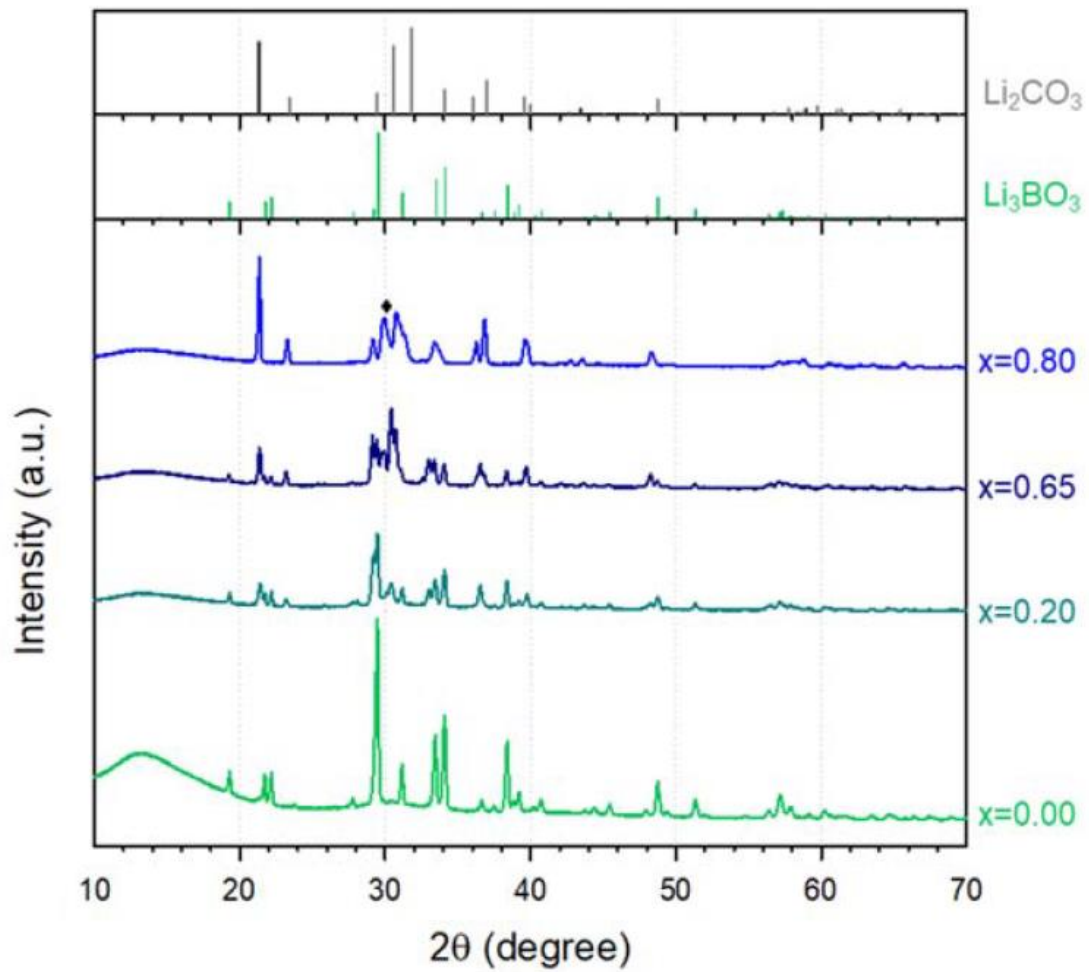| x in Li$_{3-x}$B$_{1-x}$C$_x$O$_3$	σ_{30} [S cm^{-1}]	E$_a$ [eV]
0.00	1.49 × 10^{-9}	0.60
0.20	1.18 × 10^{-7}	0.44
0.65	2.44 × 10^{-7}	0.41
0.80	6.05 × 10^{-7}	0.30

Figure 6. XRD patterns of $Li_{3-x}B_{1-x}C_xO_3$ (LBCO) and reference, Li_2CO_3 and Li_3BO_3

Table 6. Characteristics of LBO(-LCO) coatings for $LiCoO_2$

Sample	wt.% of the coatings		x in $Li_{3-x}B_{1-x}C_xO_3$	Thickness of the coating (nm)[b]	Relative surface coverage (%)[c]
	Li_3BO_3	$Li_{3-x}B_{1-x}C_xO_3$[a]			
bare	0	-	-	-	21
c-bare	0	-	-	-	0
LBO	0.05	0.06	-	1.0	-
	0.1	0.15	-	2.5	-
	0.5	0.63	-	10.4	79
LBCO	0.1	1.24	0.10	21.5	-
	0.5	1.72	0.35	29.4	87
	1.0	2.18	0.50	37.0	-
a-LBCO	0.5	1.72	0.35	29.4	88

[a] Obtained by ICP-OES, elemental analyzer, and TGA measurements. [b] Calculated based on the surface area of $LiCoO_2$, obtained by N_2 adsorption-desorption isotherm measurements (0.29 m^2 g^{-1}). [c] Obtained by LEIS measurements. Surface coverage for c-bare $LiCoO_2$ is assumed to be 0%.
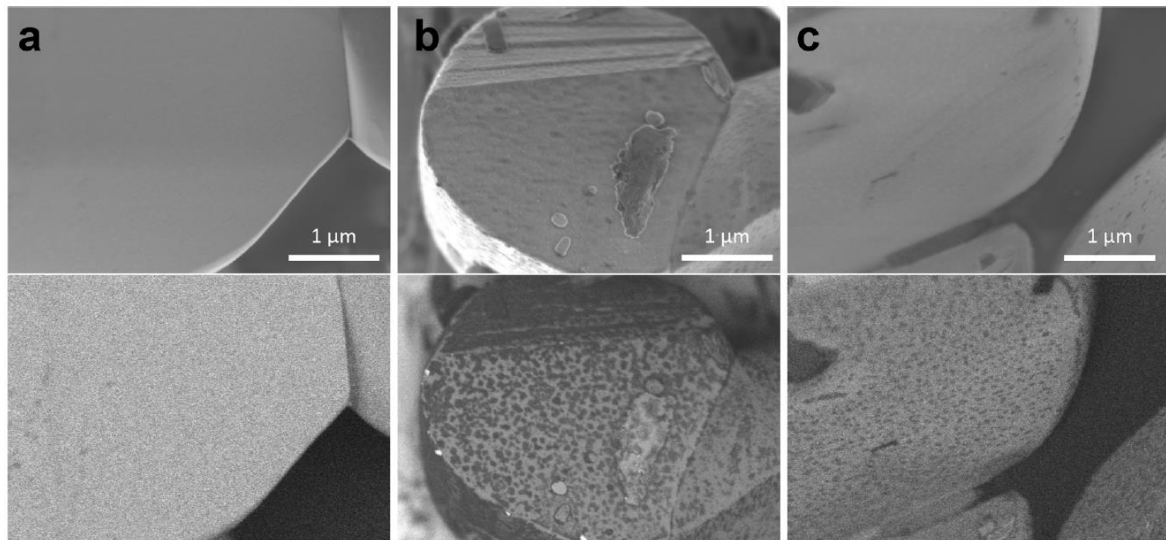
Figure 7. Characterization of c-bare (cleaned bare), LBO-coated (0.5 wt %), and LBCO-coated (0.5 wt % of LBO) LiCoO2 by electron microscopy analysis. FESEM (upper) and the corresponding BSE (lower) images for (a) c-bare, (b) LBO-coated, and (c) LBCO-coated LiCoO$_2$ particles.
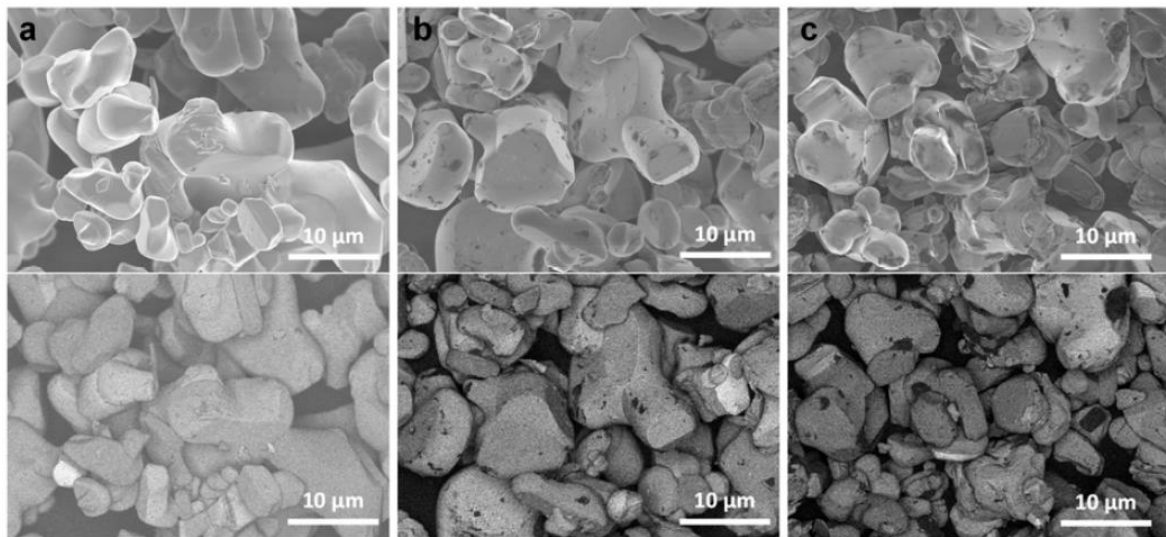
- 25 -

Figure 8. FESEM and the corresponding BSE images for a) c-bare, b) LBO-coated, and c) LBCO-coated LiCoO$_2$ powders.
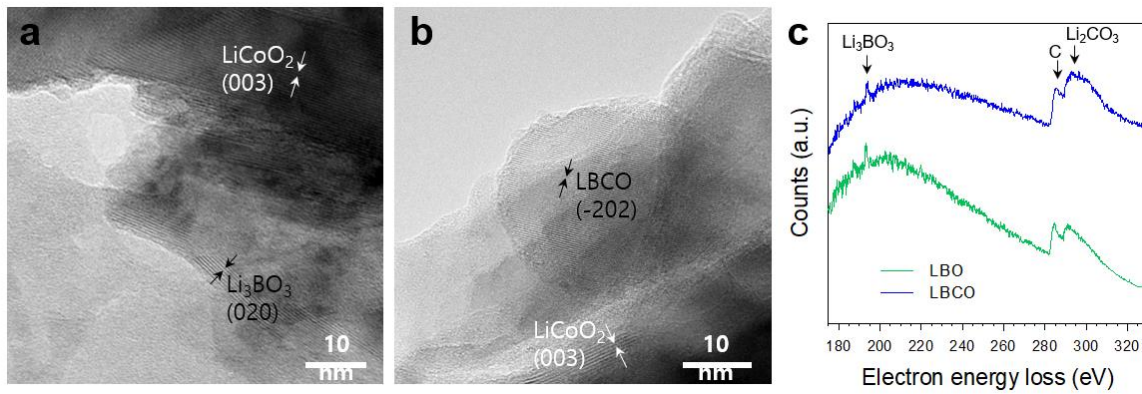
Figure 9. HRTEM images for (a)LBO- and (b)LBCO-coated LiCoO$_2$ particles. (c) EELS for LBO- and LBCO-coated LiCoO$_2$ particles. The corresponding RTEM images are provided in Figure 10.
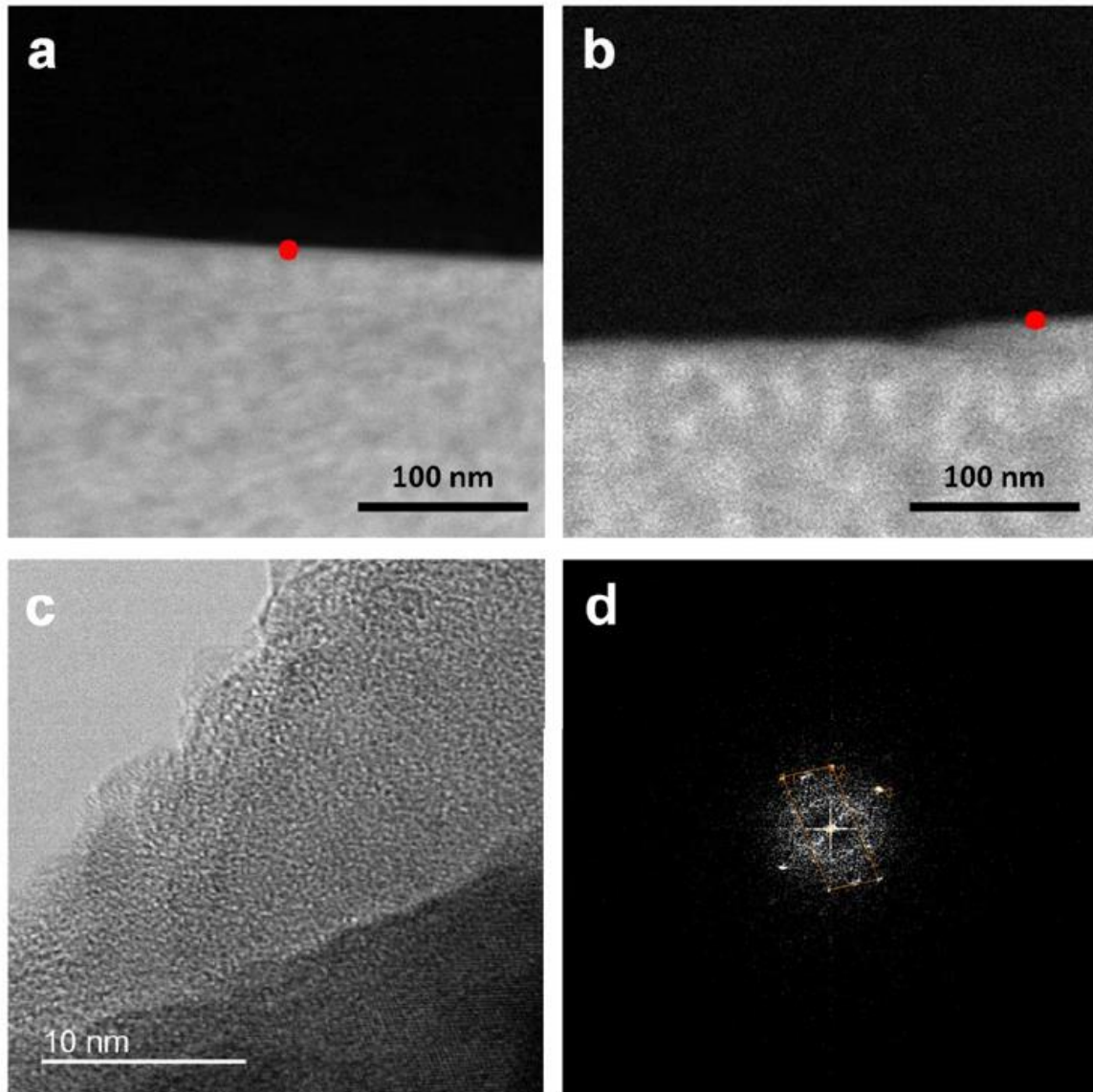
Figure 10. STEM images for a) LBO-coated and b) LBCO-coated LiCoO$_2$. The EELS data in Figure 9c correspond to the red spots in (a, b). c) TEM image for LBO-coated LiCoO$_2$ and d) its corresponding SAED pattern, which corresponds with (-1 1 1) and (1 0 1) for Li$_3$BO$_3$ (JCDPS no. 18-0718).
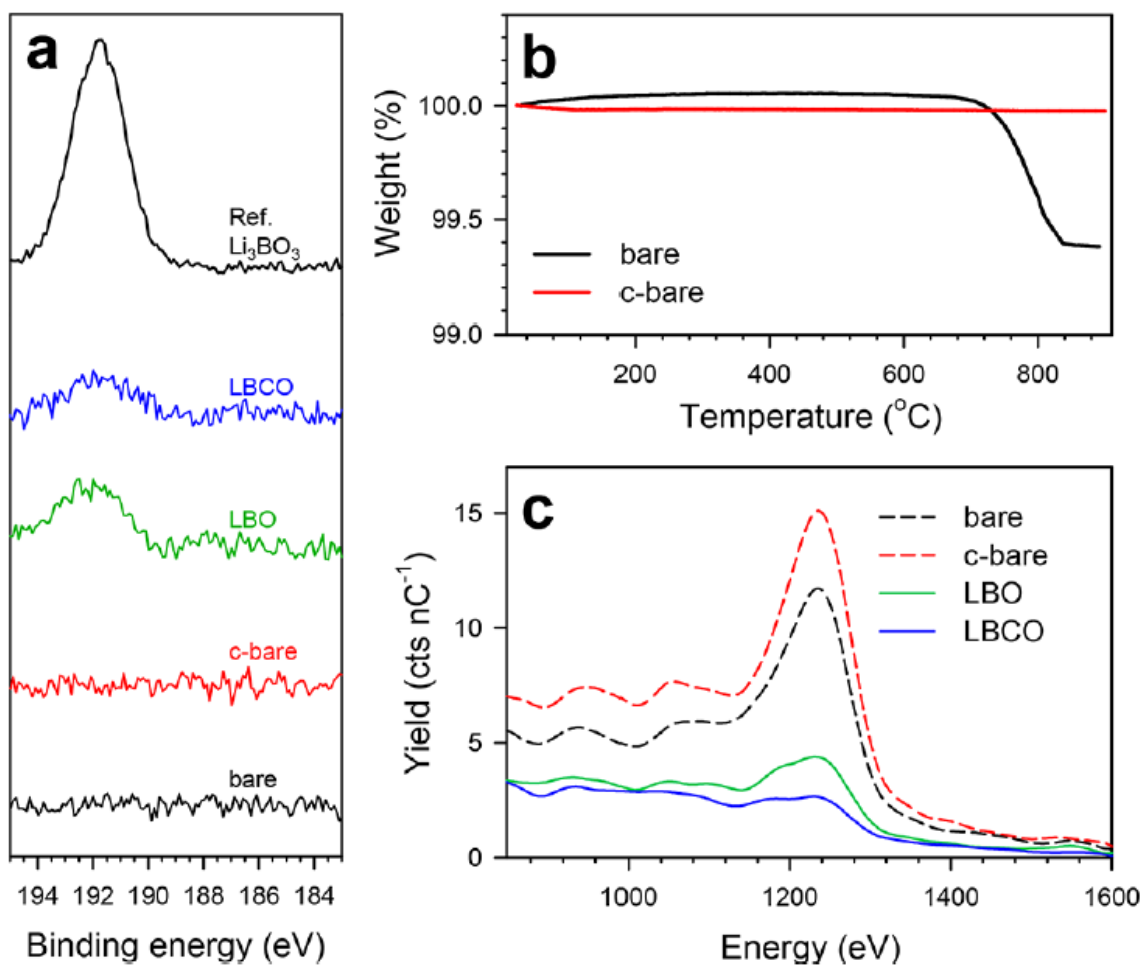
Figure 11. Characterization of bare, c-bare, LBO-coated, and LBCO-coated LiCoO$_2$. (a) XPS spectra for B 1s signals. (b) TGA profiles for bare and c-bare LiCoO$_2$ in N$_2$. (c) LEIS spectra for 5 keV Ne$^+$ incident ions.

4.3. Electrochemical characterizations

The electrochemical performances of $LiCoO_2$/Li-In all-solid-state cells at 30 °C for LBO- and LBCO-coated $LiCoO_2$, depending on the weight fraction of the coatings, are shown in Figure 12 in comparison with those for the c-bare and bare samples.   Compared with the c-bare $LiCoO_2$ samples, all the LBO-coated $LiCoO_2$ samples showed a lowered polarization in their charge-discharge voltage profiles (Figure 12a) and correspondingly higher capacities, especially at higher C-rates (Figure 12b), confirming the positive effect of the LBO coatings.   The optimal performance obtained with 0.1 wt.% of LBO may reflect that an interplay between the lowered direct contact of $LiCoO_2$-LPSCl and the non-impeded Li^+ transport through the LBO coating determines the overall kinetics.[75, 76]   The electrochemical performance was further improved by the LBCO-coating (Figure 13a, b). $LiCoO_2$ coated with LBCO with 0.5 wt.% of LBO exhibited the highest discharge capacities of 142 and 94 mA h g^{-1} at 0.2 and 2C, respectively, which are comparable to those of state-of-the-art $LiCoO_2$ electrodes in ASLBs.[11, 12, 34]   It should be noted that the LBCO coatings allow for a larger weight fraction (0.5 wt.% of LBO) than the LBO coatings (0.1 wt.%) to achieve an optimal rate capability, which can be attributed to the much higher Li^+ conductivity of LBCO compared with of LBO.   LBCO coating was also applied on c-bare $LiCoO_2$ using an aqueous solution containing LiOH, H_3BO_3, and Li_2CO_3; this sample is referred to as artificial LBCO-coated $LiCoO_2$ (a-LBCO).   Consistent with the results of LBCO-coated $LiCoO_2$, a-LBCO-coated $LiCoO_2$ also showed an excellent rate capability.   The trend of improvement, which goes in the order of bare (or c-bare), LBO-coated, and LBCO-coated samples, agrees well with the lowered polarization in the transient discharge voltage profiles obtained by galvanostatic intermittent titration technique (GITT) (Figure 14a) and the smaller interfacial resistances obtained from Nyquist plots (Figure 14b, 15, Table 7).

The cycling performances of $LiCoO_2$/Li-In all-solid-state cells at 0.2C and 30 °C using c-bare, LBO-coated, and LBCO-coated $LiCoO_2$ are shown in Figure 16.   With an upper cutoff voltage of 4.3 V (*vs.* Li/Li^+), the capacity retention for c-bare samples after 50 cycles, compared with that at the second cycle, was 88.8%.   The coatings of LBO (0.1 wt.%) and LBCO (0.5 wt.% LBO) resulted in enhancements in capacity retention: 92.2% and 93.8%, respectively.   When the upper cutoff voltage was raised to 4.5 V (*vs.* Li/Li^+), more dramatic improvements in cycling performance caused by the coating were confirmed; the capacity retentions after 25 cycles, compared with that at the fourth cycle, were 81.6%, 88.7%, and 93.8% for c-bare, LBO-coated, and LBCO-coated $LiCoO_2$, respectively.   Notably, the electrochemical performance of LBCO-coated $LiCoO_2$ for ASLBs appears to be superior to even that of the $LiNbO_3$-coated sample (Fig. S5).   From the electrochemical results, the following features are summarized: i) the rate capability and cycling performances are enhanced, from worst to best, in the order of bare (or c-bare), LBO-coated, and LBCO-coated $LiCoO_2$, ii) compared with LBO coatings, thicker coatings are possible using LBCO thanks to its higher Li^+ conductivity.
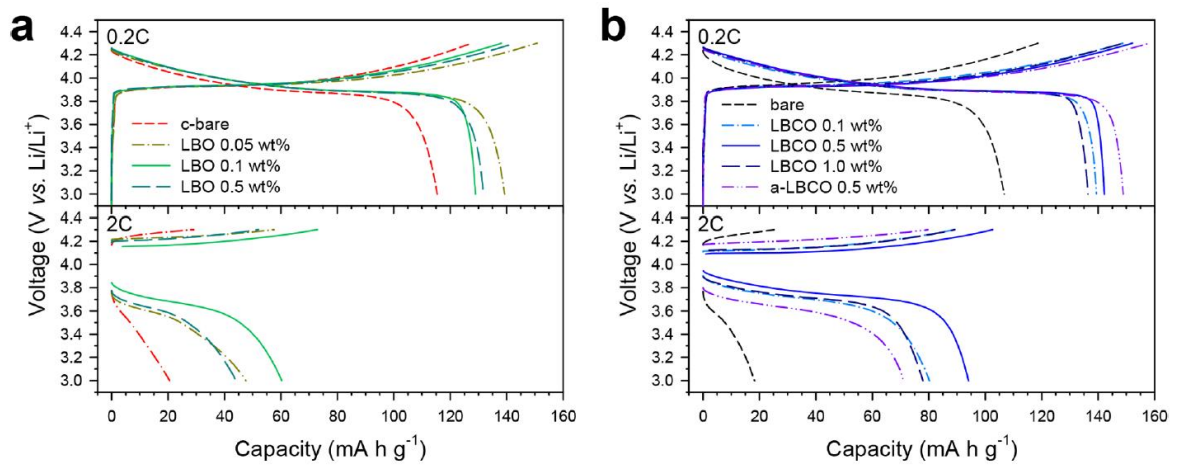
Figure 12. Electrochemical characterization of LiCoO$_2$/Li−In all-solid-state cells at 30 °C. Charge−discharge voltage profiles for (a) LBO- and (b) LBCO-coated LiCoO$_2$ varied by C-rate. The results for c-bare, bare, and a-LBCO-coated (artificial-LBCO-coated) LiCoO$_2$ are compared in (a, b).
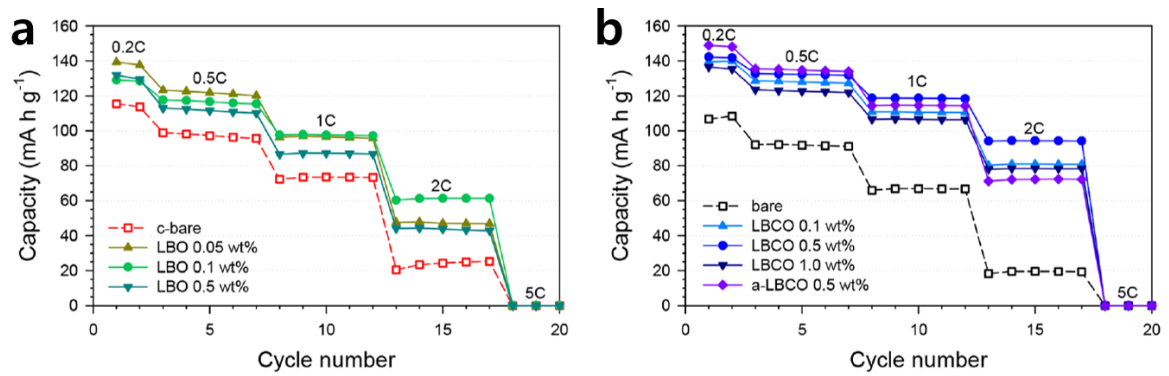
Figure 13. Electrochemical characterization of $LiCoO_2/Li-In$ all-solid-state cells at 30 °C. Rate performances for (a) LBO- and (b) LBCO-coated $LiCoO_2$. The results for c-bare, bare, and a-LBCO-coated (artificial-LBCO-coated) $LiCoO_2$ are compared in (a−b).
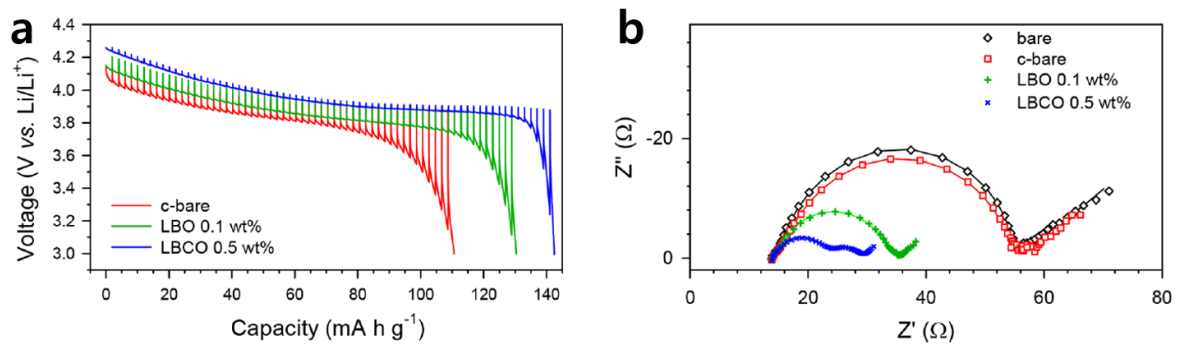
Figure 14. Electrochemical characterization of $LiCoO_2/Li-In$ all-solid-state cells at 30 °C.
(a) Transient discharge voltage profiles obtained by GITT. (b) Nyquist plots of $LiCoO_2/Li-In$ cells.
The corresponding equivalent circuit model and interfacial resistances are shown in Figure 15 and
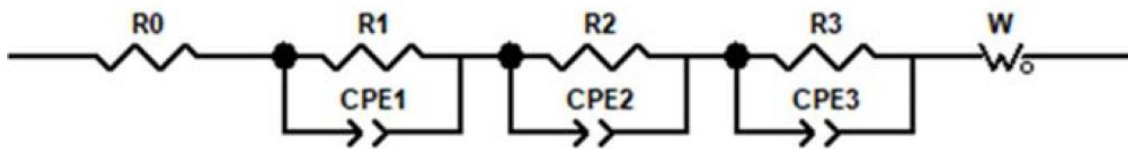Table 7, respectively.

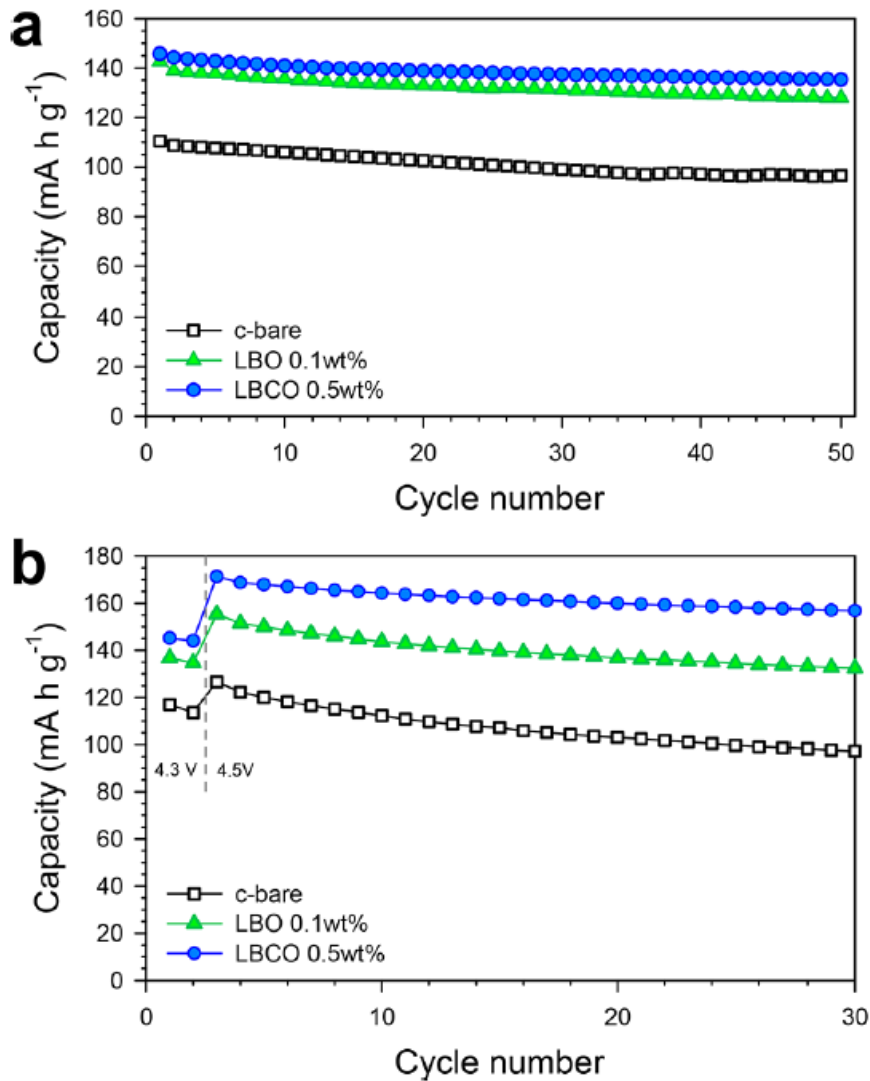**Figure 15**. Voigt-type equivalent circuit used for fitting the EIS data shown in Figure 14b.

Figure 16. Cycling performances for LiCoO₂/Li−In all-solid-state cells using c-bare, LBO-coated, and LBCO-coated LiCoO₂ at 0.2C and 30 °C. Discharge capacities as a function of the number of cycles in the voltage ranges of (a) 3.0−4.3 V (vs. Li/Li⁺) and (b) 3.0−4.5 V (vs. Li/Li⁺).

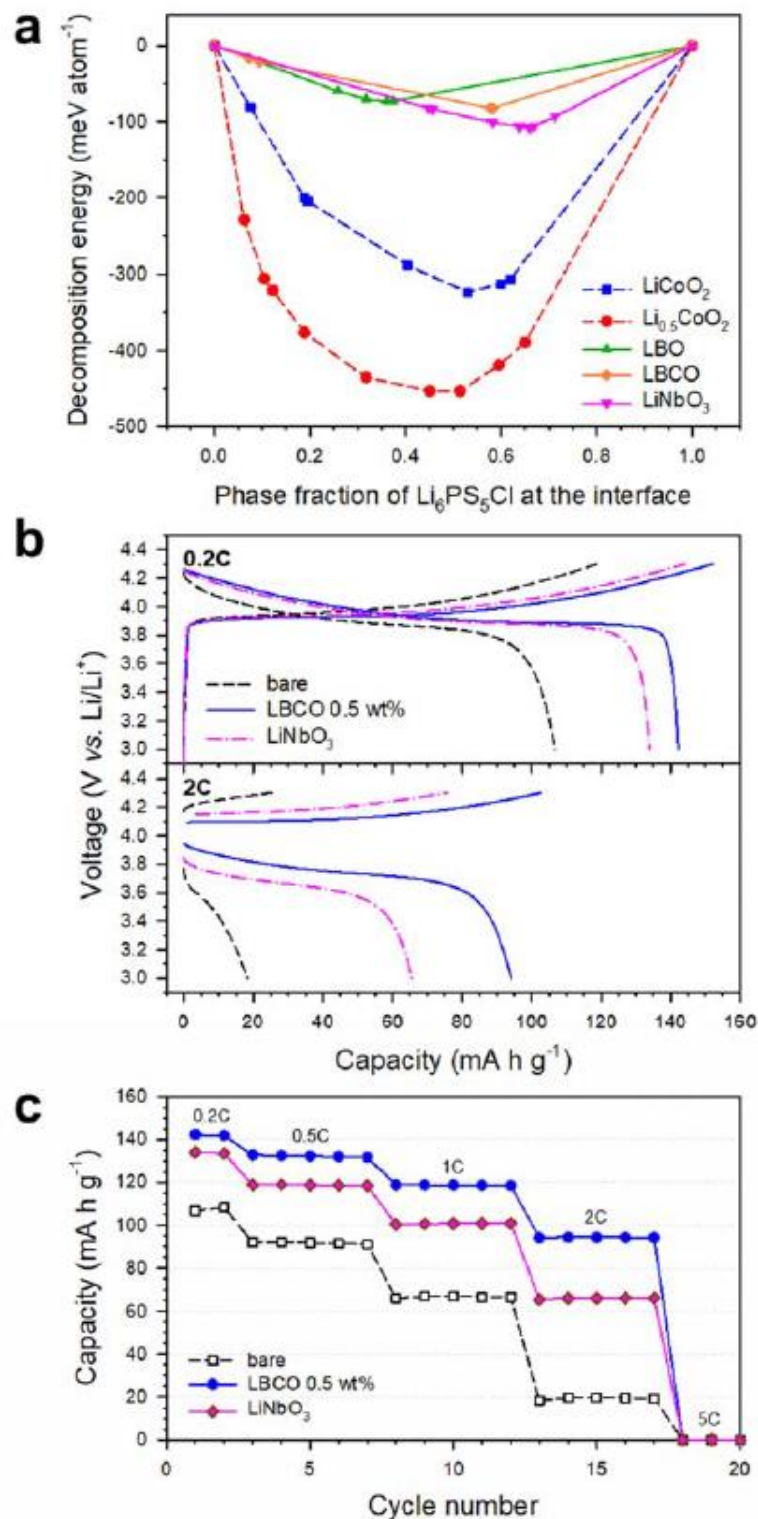**Figure 17.** Thermodynamic calculation results for LiNbO₃ and electrochemical characterization of LiNbO₃-coated LiCoO₂ (1.0 wt%). a) Calculated mutual decomposition energy of Li₆PS₅Cl with LiNbO₃. b) Charge-discharge voltage profiles at 0.2C and 2C and cycle performance for LiNbO₃-coated LiCoO₂ in LiCoO₂/Li-In all-solid-state cells at 30 °C. The results for bare, LBO-coated, and LBCO-coated LiCoO₂ are compared.

4.4. Ex-situ Surface analysis

As an attempt to gain mechanistic insights on the protective coatings on $LiCoO_2$ for ASLBs, ex-situ XPS analyses were carried out for c-bare, LBO-coated, and LBCO-coated $LiCoO_2$ electrodes before and after cycling to probe for changes at the electrode-SE interfaces. Because the mixture electrodes do not contain conducting carbon additives, any effects caused by carbon-SE interfaces could be ruled out. The signals for Co 2p, S 2p, and P 2p are shown in Figure 18-20. For the Co 2p spectra shown in Figure 18, the evolution of Co_3S_4 after cycling (shown in the deconvoluted peaks in violet) is noticeable.[77, 78] Because the physical mixture sample of c-bare $LiCoO_2/LPSCl$ does not show the signature of Co_3S_4, the formation of Co_3S_4 is suspected to be electrochemically driven, which is consistent with the observation of interatomic diffusion of Co and S at the interfaces of $LiCoO_2/Li_2S \cdot P_2S_5$ presented in a previous report.[31] Because Co_3S_4 is electronically conducting (thus non-passivating), reactions at bare $LiCoO_2/LPSCl$ interfaces occur progressively, which is detrimental to their electrochemical performance.[25, 26, 29] In stark contrast, the Co 2p signal for LBO-coated $LiCoO_2$ after cycling shows a much lower intensity for Co_3S_4. Moreover, LBCO-coated $LiCoO_2$ after cycling showed a negligible signature for Co_3S_4. This result reflects the excellent protection of $LiCoO_2$ provided by LBCO, which can be attributed to its high surface coverage (Figure 11c, Table 6) and its buffering effects, as our first principles computational results suggest (Table 4). In a consistent fashion, the suppressed evolution of Co_3S_4 after cycling from worst to best was confirmed to be in the order of c-bare, LBO-coated, and LBCO-coated $LiCoO_2$, as shown by the S 2p signals in Figure 19. As shown in the P 2p signals in Figure 20, the signature of phosphate (PO_4^{3-}, shown in the deconvoluted peaks in dark cyan) appeared for the LBO-coated sample and became more intense for the LBCO-coated one.[43, 79] The phosphate species could be derived from the electrochemical reaction of LBO or LBCO with LPSCl. In contrast to Co_3S_4, the as-formed phosphates are good electronic insulators, thus effectively passivating to inhibit the continuous decomposition of the bulk SEs.[25, 26, 29] The evolution of P_2S_{5+x} and S-S (bridging sulfur) after cycling observed in the S 2p and P 2p signals is consistent with previous reports.[43, 80, 81]

Based on the electrochemical characterization and the complementary analyses presented so far, the interface phases between cathode and SE material appear to be sensitively dependent on the coating materials used, as illustrated in Figure 21. The surfaces of bare $LiCoO_2$ are covered by the impurities, including Li_2CO_3. More importantly, the electrochemically-driven reactions between $LiCoO_2$ and LPSCl form detrimental mixed conducting interphases (MCIs), as evidenced by the observation of Co_3S_4, which shows a lack of passivating capability. The aqueous-solution coating process for LBO renders to form the LBCO layers. The high Li^+ conductivity of LBCO allows for the formation of thick and thus high-surface-coverage protective layers, which suppresses the significant decomposition

at the interface.   Moreover, the electrochemical reaction of LBCO with LPSCl enables the formation of good passivating layers comprised of phosphates.   As an overall consequence, LBCO coating on LiCoO$_2$ results in significant improvements in rate capability and durability.
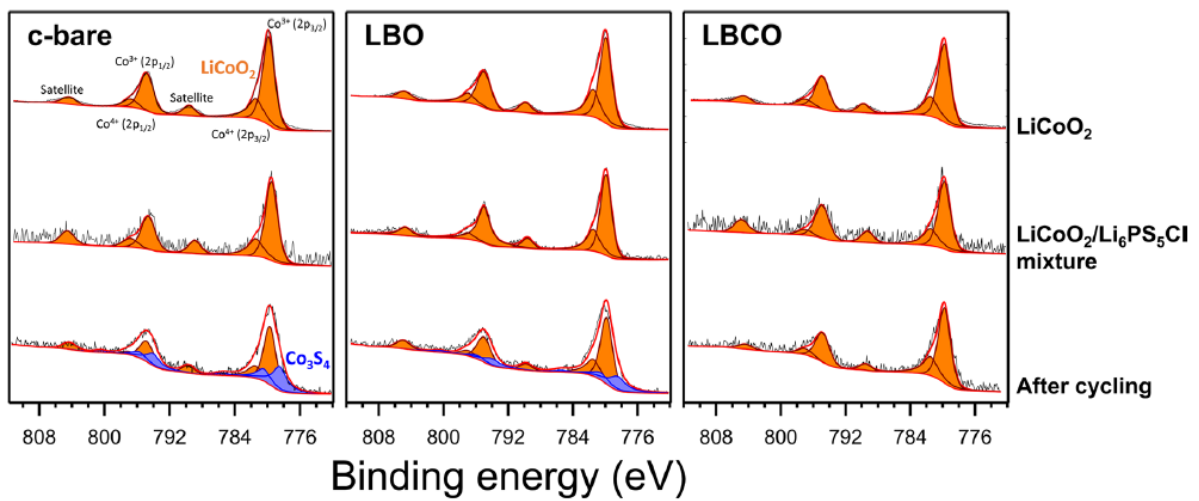
Figure 18. XPS results of Co 2p signal for c-bare, LBO-coated (0.1 wt %), and LBCO-coated (0.5 wt % of LBO) $LiCoO_2$ for pristine powders and electrodes after cycling. The data for $LiCoO_2$/SE (Li_6PS_5Cl) mixtures is also shown for comparison.

Figure 19. XPS results of S 2p signal for c-bare, LBO-coated (0.1 wt %), and LBCO-coated (0.5 wt % of LBO) LiCoO$_2$ for electrodes after cycling. The data for LiCoO$_2$/SE (Li$_6$PS$_5$Cl) mixtures is also shown for comparison.
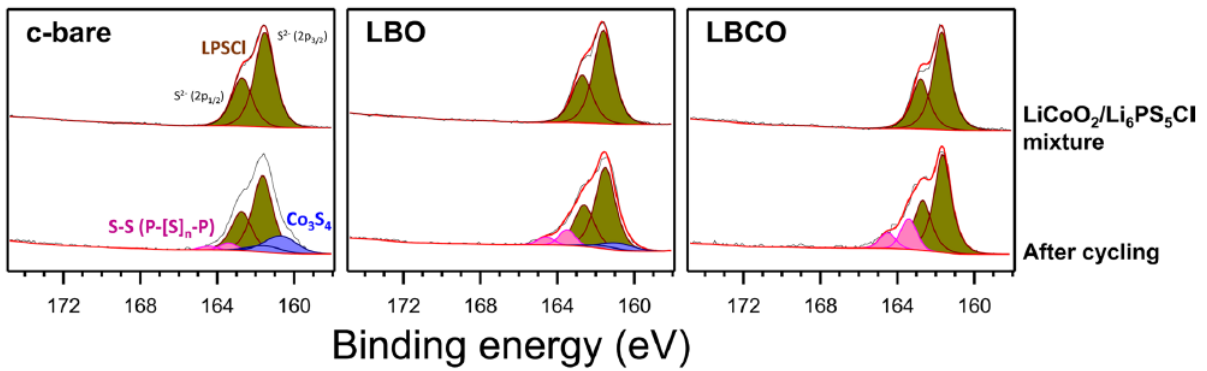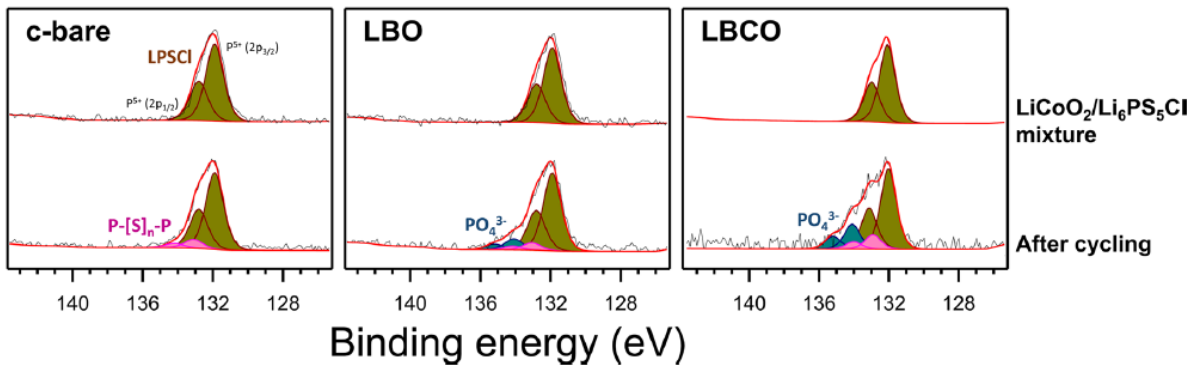
Figure 20. XPS results of P 2p signal for c-bare, LBO-coated (0.1 wt %), and LBCO-coated (0.5 wt % of LBO) $LiCoO_2$ for electrodes after cycling. The data for $LiCoO_2$/SE (Li_6PS_5Cl) mixtures is also shown for comparison.
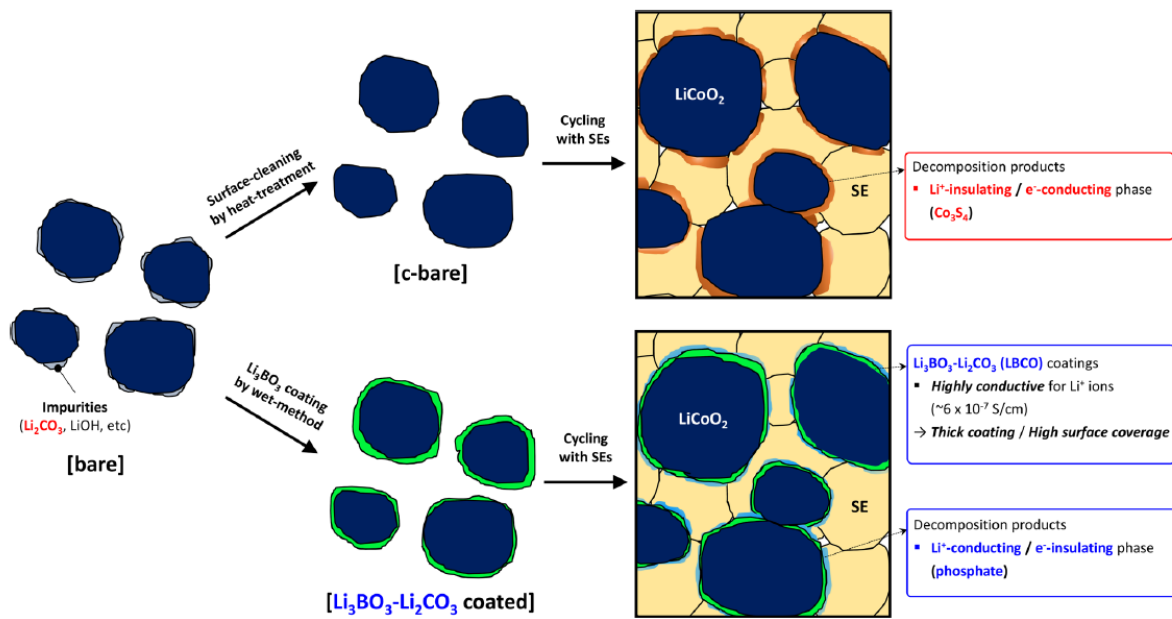
Figure 21. Schematic diagram illustrating the different interface features of bare and LBCO-coated LiCoO$_2$ in all-solid-state-cell electrodes.

5. Conclusion

In summary, a new LBCO coating process on $LiCoO_2$ for sulfide-based ASLBs via a scalable aqueous-solution protocol was rationally designed, considering the formation of an interphase between the cathode and SE materials and was demonstrated to significantly improve electrochemical performances.   Using the aforementioned aqueous LBO-solution process, the poorly Li^+-conducting surface impurity on $LiCoO_2$, Li_2CO_3, could be converted into highly Li^+-conductive LBCO (max. conductivity of 6.0×10^{-7} S cm^{-1} at 30 °C), which could protect $LiCoO_2$ with thick and high-surface-coverage layers.   More specifically, $LiCoO_2$/Li-In all-solid-state cells employing the proposed LBCO coating with 0.5 wt.% LBO showed discharge capacities of 142 and 94 mA h g^{-1} at 30 °C at 0.2C and 2C, respectively, in contrast to the discharge capacities of 107 and 18 mA h g^{-1} obtained for the ones using bare $LiCoO_2$.   From the complementary analyses by electrochemical measurements, XRD, FESEM, BSE, HRTEM, EELS, TGA, LEIS, and ex-situ XPS, it was revealed that the LBCO coatings prevent the evolution of detrimental MCIs containing Co_3S_4 and can effectively passivate the interfaces by alternatively forming phosphate-based phases.   We believe that our results provide not only an in-depth mechanistic understanding on the interfacial evolutions for ASLBs, but also open up a new avenue to rationally engineer the interfaces for practical all-solid-state technologies.

Reference

1.   Goodenough, J. B.; Kim, Y. Challenges for Rechargeable Li Batteries. *Chem. Mater.* **2010,** 22, (3), 587-603.

2.   Kalhoff, J.; Eshetu, G. G.; Bresser, D.; Passerini, S. Safer Electrolytes for Lithium-Ion Batteries: State of the Art and Perspectives. *ChemSusChem* **2015,** 8, (13), 2154-2175.

3.   Choi, J. W.; Aurbach, D. Promise and reality of post-lithium-ion batteries with high energy densities. *Nat. Rev. Mater.* **2016,** 1, 16013.

4.   Spotnitz, R.; Franklin, J. Abuse behavior of high-power, lithium-ion cells. *J. Power Sources* **2003,** 113, (1), 81-100.

5.   Jung, Y. S.; Cavanagh, A. S.; Gedvilas, L.; Widjonarko, N. E.; Scott, I. D.; Lee, S. H.; Kim, G. H.; George, S. M.; Dillon, A. C. Improved Functionality of Lithium-Ion Batteries Enabled by Atomic Layer Deposition on the Porous Microstructure of Polymer Separators and Coating Electrodes. *Adv. Energy Mater.* **2012,** 2, (8), 1022-1027.

6.   Wu, H.; Zhuo, D.; Kong, D. S.; Cui, Y. Improving battery safety by early detection of internal shorting with a bifunctional separator. *Nat. Commun.* **2014,** 5, 5193.

7.   Yamada, Y.; Usui, K.; Sodeyama, K.; Ko, S.; Tateyama, Y.; Yamada, A. Hydrate-melt electrolytes for high-energy-density aqueous batteries. *Nat. Energy* **2016**.

8.   Suo, L. M.; Hu, Y. S.; Li, H.; Armand, M.; Chen, L. Q. A new class of Solvent-in-Salt electrolyte for high-energy rechargeable metallic lithium batteries. *Nat. Commun.* **2013,** 4.

9.   Woollaston, V. New blow for Tesla: Fire in the 'world's safest electric car' began in vehicle's battery. http://www.dailymail.co.uk/sciencetech/article-2442392/New-blow-Tesla-Fire-worlds-safest-electric-car-began-vehicles-battery.html

10.   Park, K. H.; Bai, Q.; Kim, D. H.; Oh, D. Y.; Zhu, Y.; Mo, Y.; Jung, Y. S. Design Strategies, Practical Considerations, and New Solution Processes of Sulfide Solid Electrolytes for All-Solid-State Batteries. *Adv. Energy Mater.* **2018**, DOI: 10.1002/aenm.201800035.

11.   Kato, Y.; Hori, S.; Saito, T.; Suzuki, K.; Hirayama, M.; Mitsui, A.; Yonemura, M.; Iba, H.; Kanno, R. High-power all-solid-state batteries using sulfide superionic conductors. *Nat. Energy* **2016,** 1, 16030.

12.   Park, K. H.; Oh, D. Y.; Choi, Y. E.; Nam, Y. J.; Han, L.; Kim, J.-Y.; Xin, H.; Lin, F.; Oh, S. M.; Jung, Y. S. Solution-Processable Glass LiI-Li$_4$SnS$_4$ Superionic Conductors for All-Solid-State Li-Ion Batteries. *Adv. Mater.* **2016,** 28, 1874-1883.

13.   Banerjee, A.; Park, K. H.; Heo, J. W.; Nam, Y. J.; Moon, C. K.; Oh, S. M.; Hong, S.-T.; Jung, Y. S. Na$_3$SbS$_4$: A Solution Processable Sodium Superionic Conductor for All-Solid-State Sodium-Ion Batteries. *Angew. Chem. Int. Ed.* **2016,** 55, 9634-9638.

14.   Jung, Y. S.; Oh, D. Y.; Nam, Y. J.; Park, K. H. Issues and Challenges for Bulk-Type All-Solid-State Rechargeable Lithium Batteries using Sulfide Solid Electrolytes. *Israel J. Chem.* **2015,** 55, 472-485.

15.   Janek, J.; Zeier, W. G. A solid future for battery development. *Nat. Energy* **2016,** 1, 16141.

16.   Albertus, P.; Babinec, S.; Litzelman, S.; Newman, A. Status and challenges in enabling the

lithium metal electrode for high-energy and low-cost rechargeable batteries. *Nat. Energy* **2018,** 3, 16-21.

17.	Kerman, K.; Luntz, A.; Viswanathan, V.; Chiang, Y.-M.; Chen, Z. Review-Practical Challenges Hindering the Development of Solid State Li Ion Batteries. *J. Electrochem. Soc.* **2017,** 164, (7), A1731-A1744.

18.	Manthiram, A.; Yu, X.; Wang, S. Lithium battery chemistries enabled by solid-state electrolytes. *Nat. Rev. Mater.* **2017,** 2, 16103.

19.	Han, X.; Gong, Y.; Fu, K. K.; He, X.; Hitz, G. T.; Dai, J.; Pearse, A.; Liu, B.; Wang, H.; Rubloff, G.; Mo, Y.; Thangadurai, V.; Wachsman, E. D.; Hu, L. Negating interfacial impedance in garnet-based solid-state Li metal batteries. *Nat. Mater.* **2017,** 16, 572-579.

20.	Kamaya, N.; Homma, K.; Yamakawa, Y.; Hirayama, M.; Kanno, R.; Yonemura, M.; Kamiyama, T.; Kato, Y.; Hama, S.; Kawamoto, K.; Mitsui, A. A lithium superionic conductor. *Nat. Mater.* **2011,** 10, 682-686.

21.	Seino, Y.; Ota, T.; Takada, K.; Hayashi, A.; Tatsumisago, M. A sulphide lithium super ion conductor is superior to liquid ion conductors for use in rechargeable batteries. *Energy & Environ. Sci.* **2014,** 7, (2), 627-631.

22.	Doyle, M.; Fuller, T. F.; Newman, J. THE IMPORTANCE OF THE LITHIUM ION TRANSFERENCE NUMBER IN LITHIUM POLYMER CELLS. *Electrochim. Acta* **1994,** 39, (13), 2073-2081.

23.	Nam, Y. J.; Oh, D. Y.; Jung, S. H.; Jung, Y. S. Toward practical all-solid-state lithium-ion batteries with high energy density and safety: Comparative study for electrodes fabricated by dry- and slurry-mixing processes. *J. Power Sources* **2018,** 375, 93-101.

24.	Sakuda, A.; Hayashi, A.; Tatsumisago, M. Sulfide Solid Electrolyte with Favorable Mechanical Property for All-Solid-State Lithium Battery. *Sci. Rep.* **2013,** 3, 2261.

25.	Zhu, Y.; He, X.; Mo, Y. Origin of Outstanding Stability in the Lithium Solid Electrolyte Materials: Insights from Thermodynamic Analyses Based on First-Principles Calculations. *ACS Appl. Mater. Inter.* **2015,** 7, (42), 23685-23693.

26.	Wenzel, S.; Leichtweiss, T.; Weber, D. A.; Sann, J.; Zeier, W. G.; Janek, J. r. Interfacial Reactivity Benchmarking of the Sodium Ion Conductors Na_3PS_4 and Sodium β-Alumina for Protected Sodium Metal Anodes and Sodium All-Solid-State Batteries. *ACS Appl. Mater. Interfaces* **2016,** 8, (41), 28216-28224.

27.	Zhu, Y.; He, X.; Mo, Y. First principles study on electrochemical and chemical stability of solid electrolyte-electrode interfaces in all-solid-state Li-ion batteries. *J. Mater. Chem. A* **2016,** 4, (9), 3253-3266.

28.	Richards, W. D.; Miara, L. J.; Wang, Y.; Kim, J. C.; Ceder, G. Interface Stability in Solid-State Batteries. *Chem. Mater.* **2016,** 28, (1), 266-273.

29.	Tian, Y. S.; Shi, T.; Richards, W. D.; Li, J. C.; Kim, J. C.; Bo, S. H.; Ceder, G. Compatibility issues between electrodes and electrolytes in solid-state batteries. *Energy & Environ. Sci.* **2017,** 10, (5), 1150-1166.

30.   Nam, Y. J.; Jo, S. J.; Oh, D. Y.; Im, J. M.; Kim, S. Y.; Song, J. H.; Lee, Y. G.; Lee, S. Y.; Jung, Y. S. Bendable and Thin Sulfide Solid Electrolyte Film: A New Electrolyte Opportunity for Free-Standing and Stackable High-Energy All-Solid-State Lithium-Ion Batteries. *Nano Lett.* **2015,** 15, 3317-3323.

31.   Sakuda, A.; Hayashi, A.; Tatsumisago, M. Interfacial Observation between $LiCoO_2$ Electrode and Li_2S-P_2S_5 Solid Electrolytes of All-Solid-State Lithium Secondary Batteries Using Transmission Electron Microscopy. *Chem. Mater.* **2010,** 22, 949-956.

32.   Ohta, N.; Takada, K.; Zhang, L.; Ma, R.; Osada, M.; Sasaki, T. Enhancement of the high-rate capability of solid-state lithium batteries by nanoscale interfacial modification. *Adv. Mater.* **2006,** 18, 2226-2229.

33.   Takada, K. Interfacial Nanoarchitectonics for Solid-State Lithium Batteries. *Langmuir* **2013,** 29, (24), 7538-7541.

34.   Kim, D. H.; Oh, D. Y.; Park, K. H.; Choi, Y. E.; Nam, Y. J.; Lee, H. A.; Lee, S.-M.; Jung, Y. S. Infiltration of Solution-Processable Solid Electrolytes into Conventional Li-Ion-Battery Electrodes for All-Solid-State Li-Ion Batteries. *Nano Lett.* **2017,** 17, 3013-3020

35.   Liu, H. S.; Zhang, Z. R.; Gong, Z. L.; Yang, Y. Origin of deterioration for LiNiO2 cathode material during storage in air. *Electrochem. Solid State Lett.* **2004,** 7, (7), A190-A193.

36.   Xiong, X. H.; Wang, Z. X.; Yue, P.; Guo, H. J.; Wu, F. X.; Wang, J. X.; Li, X. H. Washing effects on electrochemical performance and storage characteristics of LiNi0.8Co0.1Mn0.1O2 as cathode material for lithium-ion batteries. *J. Power Sources* **2013,** 222, 318-325.

37.   Liu, W.; Oh, P.; Liu, X.; Lee, M. J.; Cho, W.; Chae, S.; Kim, Y.; Cho, J. Nickel-Rich Layered Lithium Transition-Metal Oxide for High-Energy Lithium-Ion Batteries. *Angew. Chem. Int. Ed.* **2015,** 54, (15), 4440-4457.

38.   Visbal, H.; Fujiki, S.; Aihara, Y.; Watanabe, T.; Park, Y.; Doo, S. The influence of the carbonate species on LiNi0.8Co0.05O2 surfaces for all-solid-state lithium ion battery performance. *J. Power Sources* **2014,** 269, 396-402.

39.   Ohta, N.; Takada, K.; Sakaguchi, I.; Zhang, L.; Ma, R.; Fukuda, K.; Osada, M.; Sasaki, T. LiNbO3-coated LiCoO2 as cathode material for all solid-state lithium secondary batteries. *Electrochem. Commun.* **2007,** 9, 1486-1490.

40.   Xu, X.; Takada, K.; Fukuda, K.; Ohnishi, T.; Akatsuka, K.; Osada, M.; Bui Thi, H.; Kumagai, K.; Sekiguchi, T.; Sasaki, T. Tantalum oxide nanomesh as self-standing one nanometre thick electrolyte. *Energy & Environ. Sci.* **2011,** 4, (9), 3509-3512.

41.   Woo, J. H.; Travis, J. J.; George, S. M.; Lee, S.-H. Utilization of Al2O3 Atomic Layer Deposition for Li Ion Pathways in Solid State Li Batteries. *J. Electrochem. Soc.* **2015,** 162, (3), A344-A349.

42.   Ito, Y.; Sakurai, Y.; Yubuchi, S.; Sakuda, A.; Hayashi, A.; Tatsumisago, M.; . Application of $LiCoO_2$ Particles Coated with Lithium Ortho-Oxosalt Thin Films to Sulfide-Type All-Solid-State Lithium Batteries Batteries and Energy Storage *J. Electrochem. Soc.* **2015,** 162, (8), A1610.

43.   Auvergniot, J.; Cassel, A.; Ledeuil, J. B.; Viallet, V.; Seznec, V.; Dedryvere, R. Interface Stability of Argyrodite Li6PS5Cl toward LiCoO2, LiNi1/3Co1/3Mn1/3O2, and LiMn2O4 in Bulk All-

Solid-State Batteries. *Chem. Mater.* **2017,** 29, (9), 3883-3890.

44.		Koerver, R.; Aygün, I.; Leichtweiß, T.; Dietrich, C.; Zhang, W.; Binder, J. O.; Hartmann, P.; Zeier, W. G.; Janek, J. Capacity Fade in Solid-State Batteries: Interphase Formation and Chemomechanical Processes in Nickel-Rich Layered Oxide Cathodes and Lithium Thiophosphate Solid Electrolytes. *Chem. Mater.* **2017,** 29, 5574-5582.

45.		Shannon, R. D.; Taylor, B. E.; English, A. D.; Berzins, T. NEW LI SOLID ELECTROLYTES. *Electrochimica Acta* **1977,** 22, (7), 783-796.

46.		Ohta, S.; Komagata, S.; Seki, J.; Saeki, T.; Morishita, S.; Asaoka, T. All-solid-state lithium ion battery using garnet-type oxide and Li3BO3 solid electrolytes fabricated by screen-printing. *J. Power Sources* **2013,** 238, 53-56.

47.		Ohta, S.; Seki, J.; Yagi, Y.; Kihira, Y.; Tani, T.; Asoka, T. Co-sinterable lithium garnet-type oxide electrolyte with cathode for all-solid-state lithium ion battery. *J. Power Sources* **2014,** 265, 40-44.

48.		Okumura, T.; Takeuchi, T.; Kobayashi, H. All-solid-state lithium-ion battery using Li2.2C0.8B0.2O3 electrolyte. *Solid State Ionics* **2016,** 288, 248-252.

49.		Nagao, K.; Hayashi, A.; Tatsumisago, M. Mechanochemical synthesis and crystallization of Li3BO3-Li2CO3 glass electrolytes. *J. Ceram. Soc. Jpn.* **2016,** 124, (9), 915-919.

50.		Park, K.; Yu, B. C.; Jung, J. W.; Li, Y. T.; Zhou, W. D.; Gao, H. C.; Son, S.; Goodenough, J. B. Electrochemical Nature of the Cathode Interface for a Solid-State Lithium-Ion Battery: Interface between LiCoO2 and Garnet-Li7La3Zr2O12. *Chem. Mater.* **2016,** 28, (21), 8051-8059.

51.		Yada, C.; Lee, C. E.; Laughman, D.; Hannah, L.; Iba, H.; Hayden, B. E. A high-throughput approach developing lithium-niobium-tantalum oxides as electrolyte/cathode interlayers for high-voltage all-solid-state lithium batteries. *Journal of the Electrochemical Society* **2015,** 162, (4), A722-A726.

52.		Ito, S.; Fujiki, S.; Yamada, T.; Aihara, Y.; Park, Y.; Kim, T. Y.; Baek, S. W.; Lee, J. M.; Doo, S.; Machida, N. A rocking chair type all-solid-state lithium ion battery adopting Li $_2$O-ZrO$_2$ coated LiNi$_{0.8}$Co$_{0.15}$Al $_{0.05}$O$_2$ and a sulfide based electrolyte. *Journal of Power Sources* **2014,** 248, 943-950.

53.		Tarascon, J. M.; Armand, M. Issues and challenges facing rechargeable lithium batteries. *Nature* **2001,** 414, (6861), 359-367.

54.		Goodenough, J. B.; Park, K.-S. The Li-Ion Rechargeable Battery: A Perspective. *Journal of the American Chemical Society* **2013,** 135, (4), 1167-1176.

55.		Manthiram, A.; Yu, X.; Wang, S. Lithium battery chemistries enabled by solid-state electrolytes. *Nature Reviews Materials* **2017,** 2, 16103.

56.		Zhang, B.; Tan, R.; Yang, L.; Zheng, J.; Zhang, K.; Mo, S.; Lin, Z.; Pan, F. Mechanisms and properties of ion-transport in inorganic solid electrolytes. *Energy Storage Materials* **2018,** 10, 139-159.

57.		Wang, Y.; Richards, W. D.; Ong, S. P.; Miara, L. J.; Kim, J. C.; Mo, Y.; Ceder, G. Design principles for solid-state lithium superionic conductors. *Nature Materials* **2015,** 14, 1026.

58.   Bates, J. B.; Dudney, N. J.; Neudecker, B.; Ueda, A.; Evans, C. D. Thin-film lithium and lithium-ion batteries. *Solid State Ionics* **2000,** 135, (1), 33-45.

59.   Patil, A.; Patil, V.; Wook Shin, D.; Choi, J.-W.; Paik, D.-S.; Yoon, S.-J. Issue and challenges facing rechargeable thin film lithium batteries. *Materials Research Bulletin* **2008,** 43, (8), 1913-1942.

60.   Wang, B.; Bates, J. B.; Hart, F. X.; Sales, B. C.; Zuhr, R. A.; Robertson, J. D. Characterization of Thin-Film Rechargeable Lithium Batteries with Lithium Cobalt Oxide Cathodes. *Journal of The Electrochemical Society* **1996,** 143, (10), 3203-3213.

61.   Seino, Y.; Ota, T.; Takada, K.; Hayashi, A.; Tatsumisago, M. A sulphide lithium super ion conductor is superior to liquid ion conductors for use in rechargeable batteries. *Energy & Environmental Science* **2014,** 7, (2), 627-631.

62.   Sakuda, A.; Hayashi, A.; Tatsumisago, M. Sulfide Solid Electrolyte with Favorable Mechanical Property for All-Solid-State Lithium Battery. *Scientific Reports* **2013,** 3, 2261.

63.   Ohta, S.; Kobayashi, T.; Asaoka, T. High lithium ionic conductivity in the garnet-type oxide Li7−X La3(Zr2−X, NbX)O12 (X=0–2). *Journal of Power Sources* **2011,** 196, (6), 3342-3345.

64.   Han, F.; Gao, T.; Zhu, Y.; Gaskell, K. J.; Wang, C. A Battery Made from a Single Material. *Advanced Materials* **2015,** 27, (23), 3473-3483.

65.   Haruyama, J.; Sodeyama, K.; Han, L.; Takada, K.; Tateyama, Y. Space–Charge Layer Effect at Interface between Oxide Cathode and Sulfide Electrolyte in All-Solid-State Lithium-Ion Battery. *Chemistry of Materials* **2014,** 26, (14), 4248-4255.

66.   Trevey, J. E.; Rason, K. W.; Stoldt, C. R.; Lee, S.-H. Improved Performance of All-Solid-State Lithium-Ion Batteries Using Nanosilicon Active Material with Multiwalled-Carbon-Nanotubes as a Conductive Additive. *Electrochemical and Solid-State Letters* **2010,** 13, (11), A154-A157.

67.   Aboulaich, A.; Bouchet, R.; Delaizir, G.; Seznec, V.; Tortet, L.; Morcrette, M.; Rozier, P.; Tarascon, J.-M.; Viallet, V.; Dollé, M. A New Approach to Develop Safe All-Inorganic Monolithic Li-Ion Batteries. *Advanced Energy Materials* **2011,** 1, (2), 179-183.

68.   Jain, A.; Ong, S. P.; Hautier, G.; Chen, W.; Richards, W. D.; Dacek, S.; Cholia, S.; Gunter, D.; Skinner, D.; Ceder, G.; Persson, K. A. Commentary: The Materials Project: A materials genome approach to accelerating materials innovation. *APL Materials* **2013,** 1, (1), 011002.

69.   Han, F.; Yue, J.; Chen, C.; Zhao, N.; Fan, X.; Ma, Z.; Gao, T.; Wang, F.; Guo, X.; Wang, C. Interphase Engineering Enabled All-Ceramic Lithium Battery. *Joule* **2018**.

70.   Schreifels, J. A.; Maybury, P. C.; Swartz, W. E. X-RAY PHOTOELECTRON-SPECTROSCOPY OF NICKEL BORIDE CATALYSTS - CORRELATION OF SURFACE-STATES WITH REACTION-PRODUCTS IN THE HYDROGENATION OF ACRYLONITRILE. *J. Catal.* **1980,** 65, (1), 195-206.

71.   Lin, F.; Markus, I. M.; Doeff, M. M.; Xin, H. L. L. Chemical and Structural Stability of Lithium-Ion Battery Electrode Materials under Electron Beam. *Sci. Rep.* **2014,** 4.

72.   Kim, J. W.; Lee, H. G. Thermal and carbothermic decomposition of Na2CO3 and Li(2)CO3. *Metall. Mater. Trans. B* **2001,** 32, (1), 17-24.

73.   Jung, S. H.; Kim, D. H.; Brüner, P.; Lee, H.; Hah, H. J.; Kim, S. K.; Jung, Y. S. Extremely

conductive RuO_2-coated $LiNi_{0.5}Mn_{1.5}O_4$ for lithium-ion batteries. *Electrochim. Acta* **2017,** 232, 236–243.

74.	Kaufmann, E. N.; Brongersma, H. H., *Characterization of Materials*. John Wiley and Sons, Inc.: 2012.

75.	Jung, Y. S.; Cavanagh, A. S.; Riley, L. A.; Kang, S. H.; Dillon, A. C.; Groner, M. D.; George, S. M.; Lee, S. H. Ultrathin Direct Atomic Layer Deposition on Composite Electrodes for Highly Durable and Safe Li-Ion Batteries. *Adv. Mater.* **2010,** 22, (19), 2172-2176.

76.	Zhu, C.; Usiskin, R. E.; Yu, Y.; Maier, J. The nanoscale circuitry of battery electrodes. *Science* **2017,** 358, 1400.

77.	Gu, W. L.; Hu, L. Y.; Hong, W.; Jia, X. F.; Li, J.; Wang, E. K. Noble-metal-free Co3S4-S/G porous hybrids as an efficient electrocatalyst for oxygen reduction reaction. *Chem. Sci.* **2016,** 7, (7), 4167-4173.

78.	Du, J.; Zhang, T.; Xing, J. L.; Xu, C. L. Hierarchical porous Fe3O4/Co3S4 nanosheets as an efficient electrocatalyst for the oxygen evolution reaction. *J. Mater. Chem. A* **2017,** 5, (19), 9210-9216.

79.	Kozen, A. C.; Pearse, A. J.; Lin, C. F.; Noked, M.; Rubloff, G. W. Atomic Layer Deposition of the Solid Electrolyte LiPON. *Chem. Mater.* **2015,** 27, (15), 5324-5331.

80.	Hakari, T.; Deguchi, M.; Mitsuhara, K.; Ohta, T.; Saita, K.; Orikasa, Y.; Uchimoto, Y.; Kowada, Y.; Hayashi, A.; Tatsumisago, M. Structural and Electronic-State Changes of a Sulfide Solid Electrolyte during the Li Deinsertion-Insertion Processes. *Chem. Mater.* **2017,** 29, (11), 4768-4774.

81.	Auvergniot, J.; Cassel, A.; Foix, D.; Viallet, V.; Seznec, V.; Dedryvere, R. Redox activity of argyrodite Li6PS5Cl electrolyte in all-solid-state Li-ion battery: An XPS study. *Solid State Ionics* **2017,** 300, 78-85.

82.	Jung, S. H.; Oh, K. B.; Nam, Y. J.; Oh, D. Y. Pillip, B.; Kang, K. S.; Jung, Y. S. Li_3BO_3-Li_2CO_3: Rationally Designed Buffering Phase for Sulfide All-Solid-State Li-Ion Batteries. *Chem. Mater.* **2018**, 30, 8190-8200

Permission

Title:	Lithium battery chemistries enabled by solid-state electrolytes	Logged in as: Sung Hoo Jung
Author:	Arumugam Manthiram, Xingwen Yu, Shaofei Wang	Account #: 3001452163
Publication:	Nature Reviews Materials	LOGOUT
Publisher:	Springer Nature	
Date:	Feb 14, 2017	
Copyright © 2017, Springer Nature		

Order Completed

Thank you for your order.

This Agreement between Mr. Sung Hoo Jung ("You") and Springer Nature ("Springer Nature") consists of your license details and the terms and conditions provided by Springer Nature and Copyright Clearance Center.

Your confirmation email will contain your order number for future reference.

printable details

|	
License Number	4586591172446
License date	May 12, 2019
Licensed Content Publisher	Springer Nature
Licensed Content Publication	Nature Reviews Materials
Licensed Content Title	Lithium battery chemistries enabled by solid-state electrolytes
Licensed Content Author	Arumugam Manthiram, Xingwen Yu, Shaofei Wang
Licensed Content Date	Feb 14, 2017
Licensed Content Volume	2
Licensed Content Issue	4
Type of Use	Thesis/Dissertation
Requestor type	non-commercial (non-profit)
Format	print and electronic
Portion	figures/tables/illustrations
Number of figures/tables/illustrations	1
High-res required	no
Will you be translating?	no
Circulation/distribution	<501
Author of this Springer Nature content	no
Title	Interfacial Evolution and Engineering on LiMO2(M = Co, Ni, Mn) Positive Electrodes for All-Solid-State Li-Ion Batteries Using Sulfide Solid Electrolytes
Institution name	n/a
Expected presentation date	Sep 2019
Portions	Figure 2
Requestor Location	Mr. Sung Hoo Jung Seoul, Republic of Korea FTC 803, Wangsimni-ro, Seongdong-gu
	Seoul, Seoul 04763 Korea, Republic Of Attn: Mr. Sung Hoo Jung
Total	0.00 USD
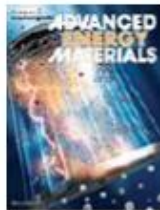
Title: Design Strategies, Practical Considerations, and New Solution Processes of Sulfide Solid Electrolytes for All-Solid-State Batteries

Author: Kern Ho Park, Qiang Bai, Dong Hyeon Kim, et al

Publication: Advanced Energy Materials

Publisher: John Wiley and Sons

Date: Apr 23, 2018

© WILEY-VCH Verlag GmbH & Co. KGaA, Weinheim

Order Completed

Thank you for your order.

This Agreement between Mr. Sung Hoo Jung ("You") and John Wiley and Sons ("John Wiley and Sons") consists of your license details and the terms and conditions provided by John Wiley and Sons and Copyright Clearance Center.

Your confirmation email will contain your order number for future reference.

printable details

License Number	4586570223488
License date	May 12, 2019
Licensed Content Publisher	John Wiley and Sons
Licensed Content Publication	Advanced Energy Materials
Licensed Content Title	Design Strategies, Practical Considerations, and New Solution Processes of Sulfide Solid Electrolytes for All-Solid-State Batteries
Licensed Content Author	Kern Ho Park, Qiang Bai, Dong Hyeon Kim, et al
Licensed Content Date	Apr 23, 2018
Licensed Content Volume	8
Licensed Content Issue	18
Licensed Content Pages	24
Type of use	Dissertation/Thesis
Requestor type	University/Academic
Format	Print and electronic
Portion	Figure/table
Number of figures/tables	2
Original Wiley figure/table number(s)	Figure 1
Will you be translating?	No
Title of your thesis / dissertation	Interfacial Evolution and Engineering on LiMO2(M = Co, Ni, Mn) Positive Electrodes for All-Solid-State Li-Ion Batteries Using Sulfide Solid Electrolytes
Expected completion date	Sep 2019
Expected size (number of pages)	2
Requestor Location	Mr. Sung Hoo Jung Seoul, Republic of Korea FTC 803, Wangsimni-ro, Seongdong-gu Seoul, Seoul 04763 Korea, Republic Of Attn: Mr. Sung Hoo Jung
Publisher Tax ID	EU826007151
Total	0.00 USD

Copyright Clearance Center

RightsLink

ACS Publications
Most Trusted. Most Cited. Most Read.

Title: Li3BO3–Li2CO3: Rationally Designed Buffering Phase for Sulfide All-Solid-State Li-Ion Batteries

Author: Sung Hoo Jung, Kyungbae Oh, Young Jin Nam, et al

Publication: Chemistry of Materials

Publisher: American Chemical Society

Date: Nov 1, 2018

Copyright © 2018, American Chemical Society

PERMISSION/LICENSE IS GRANTED FOR YOUR ORDER AT NO CHARGE